Transient tyre models with a flexible carcass

N.B. When citing this work, cite the original published paper.

(article starts on next page)

Transient tyre models with a flexible carcass

Luigi Romano[*a], Fredrik Bruzelius[a], and Bengt Jacobson[a]

[a]Department of Mechanics and Maritime Sciences, Chalmers University of Technology, Hörsalsvägen 7A, 412 96 Gothenburg, Sweden

Abstract

The accuracy of transient tyre models may be largely improved by considering the flexibility of the tyre carcass. Several formulations, whereby the unsteady behaviour of the tyre is approximated using linear or nonlinear systems of ordinary differential equations (ODEs), are already available in the literature. However, when the tread behaviour is described using a distributed representation, that is, in terms of partial differential equations (PDEs), the inclusion of even the simplest model to represent the deformation of the tyre carcass leads to rather involved PDE or interconnected PDE-ODE systems, with nonlocal and boundary terms. Such descriptions require detailed analyses that have not been attempted so far. Therefore, this paper investigates the salient properties of the classic brush and LuGre-brush models considering the effect of a flexible carcass. For both formulations, the existence and uniqueness of the solution are discussed. For the standard version of the brush models, a closed-form solution is provided under the assumption of vanishing sliding, whereas the case of limited friction is explored only qualitatively. Concerning the LuGre-brush variant, the preliminary intuition gained from the analysis of the distributed representation is effectively used to develop approximated lumped formulations to be used in control-oriented applications.

Keywords

Tyre modelling; distributed tyre models; brush model; LuGre-brush model; transient tyre dynamics; tyre carcass

1 Introduction

The transient dynamics of the tyre is a rather intriguing and elusive phenomenon [1–3], involving several interconnected aspects. Amongst the external stimuli that may excite nonstationary behaviours in the tyre-wheel assembly there are, for example, time-varying slip and spin inputs [4, 5], unsteady effects due to the compliance of the tyre tread and carcass, and even abrupt discontinuities in the available friction at the tyre-road interface. In order to synthesise and implement *ad-hoc* algorithms and strategies for vehicle state estimation and control [6–21], it is crucial to rely on simple and plausible physical models, capable of explaining at least qualitatively all the above-mentioned processes, and their influence upon the transient generation of tyre forces and moments [2, 22, 23].

In the dedicated literature, there is an abundance of pragmatic models that approximate the transient dynamics of the tyre using a system of ordinary differential equations (ODEs), describing the time-evolution of the forces and moment depending upon the slip and spin inputs. Such representations include primarily the *single contact point* models [24–32], the *two-regime* formulation [4, 33, 34], and the lumped approximation of the LuGre-brush models [35–41]. In this context, the single contact point models constitute a standard approach when it comes to full vehicle dynamics simulations, since they can be easily integrated with Pacejka's Magic Formula (MF) [1, 42] or other empirical steady-state tyre formulae. The basic assumption of the single contact point formulation is that the tyre dynamics may be approximated as that of a linear system, whose main parameter is the so-called *relaxation length*. This is identified as the distance that the tyre needs to travel to develop 63% of the steady-state forces. In the single contact point approximation, nonstationary effects connected with the deformation of tread particles are systematically neglected, and the carcass element is completely responsible for the transient

---

[*]Corresponding author. Email: luigi.romano@chalmers.se.

process of generation of tyre forces and moment. This pragmatic approach leads to a very straightforward model, which generally shows a good agreement with experimental evidence and – combined with MF, which is currently able to take into account physical phenomena connected to tyre inflation pressure, temperature and wear [43–46] – can also handle the presence of large camber angles and steering speeds. On the same lines, the two-regime [33] formulation consists of a relatively novel description that mimics the dual nature of the tyre by a series system behaving as a spring at low rolling speed and as a damper at high speeds [4, 33, 34]. However, as opposed to the single contact point formulation, the two-regime models describe the tyre dynamics by means of a nonlinear system of ODEs directly in terms of forces and moment, and also take explicitly into account transient effects connected with the deformation of the tyre tread. Finally, the lumped LuGre-brush models [35–41], based on the LuGre friction theory proposed by Canudas-de-Wit and Åström [47], condense the distributed dynamics of the tyre tread using an averaged or global frictional state, which is able to accurately capture nonstationary phenomena. However, this formulation does not include the contribution of a compliant carcass.

On the other hand, three main formulations may be identified in the existing literature concerning distributed representations of the tyre, that is, modelled in terms of partial differential equations (PDEs). The first analytical description consists of the *stretched string* models and their derivations, which were first developed by Schlippe and Segel [48, 49] to investigate the lateral response of the tyre when subjected to small slip inputs. In these descriptions, the tyre carcass is assimilated to an undamped string of infinite length, undergoing elastic deformation during the rolling at constant velocity. Whilst the original variant of the stretched string model did not account for the deformation of the tyre tread, and was limited to the linear case, both Pacejka and Higuchi enhanced the model by integrating the description with tread elements [50] and limited friction available inside the contact patch [24, 25]. However, such extensions were mainly restricted to the condition of steady-state rolling. Other improved versions consider the compliance of the tyre in the longitudinal direction [51–53], the exact coupled nonlinear kinematics of the rubber particles contacting the ground and the vehicle motion [54–60], and the presence of limited friction inside the tyre contact patch even in transient conditions [61–63], according to the classic Coulomb-Amontons assumption [64–73]. A simpler description, the brush models [1, 2, 74] approximate the continuum of the tyre tread by means of infinitesimal bristles attached to the tyre-wheel systems, assumed infinitely rigid. The resulting mathematical formalisation consists of two linear transport equations [1], which model the time-varying deformation of the bristles according to the Eulerian approach. The brush models have only been recently adopted to investigate the transient dynamics of the tyres in some works by the authors [4, 34, 75, 76] and by Guiggiani [2], where numerous extensions have been introduced. For example, the effect of large spin slips has been considered in [34, 75–78], where the analysis has permitted to identify and exhaustively explain the separate contributions of the camber and turn spin. On the other hand, in his authoritative and elegant book, Guiggiani [2] has firstly attempted a rigorous analysis of the nonstationary phenomena connected with the presence of a flexible carcass. A major drawback of the brush theory is that a simple structure for its governing PDEs is only retained under the assumption of vanishing sliding, which corresponds to infinite friction available inside the contact patch. This aspect is intimately connected with the Coulomb-Amontons friction model, which discriminates between stick and slip behaviours. In this context, the technical difficulties encountered when attempting a rigorous analysis of the model make the formulation unsuitable for control purposes. These limitations are instead overcome by the LuGre-brush description, which postulates a different friciton model, especially conceived to facilitate the design and synthesis of controllers and estimators for automotive applications.

Excluding some isolated contributions [2, 34], the mathematical analysis of both the standard and modified LuGre-based versions of the brush models has been so far restricted to the case of rigid carcass. Indeed, when considering a compliant carcass element (traditionally modelled as a linear spring), additional quantities – involving nonlocal and boundary terms – appear in the governing PDEs of these models, which make the investigation substantially more complicated. However, in most applications, the transient effects connected with the distortion of the tyre carcass are a preponderant over those induced by the tread particles, and hence cannot be disregarded. Therefore, the aim of this paper is to analyse the transient dynamics of the distributed brush and LuGre-brush tyre models when taking into account the flexibility of the tyre carcass. In this context, it should be clarified that the carcass model considered in the present investigation is the simplest possible, that is, a linear spring that only undergoes tangential deformations, whereas twisting and bending effects are systematically neglected. Inertial contributions and damping phenomena are also disregarded. This choice is legitimated by the complexity of the mathematical analysis conducted in the paper. Moreover, spring-like approximations are also incorporated into more sophisticated descriptions, like the famous *rigid-ring* model [79].

The remainder of the manuscript is organised as follows. Section 2 introduces the governing equations

of the brush and LuGre-brush tyre models, recapitulates their essential assumptions and simplifications, and states the corresponding boundary (BCs) and initial conditions (ICs). Section 3 is dedicated to the unsteady version of the classic brush theory. The salient results concerning the model with rigid carcass are first summarised. Then, the effect of a compliant carcass is discussed quantitatively and qualitatively for the cases of vanishing sliding (for which a closed-form solution is also derived) and limited friction. In Sect. 4, the unsteady dynamics of the tyre is explored within the theoretical framework of the LuGre-brush models. Two different systems of ODEs and interconnected PDE-ODEs are derived, depending on some specific conditions satisfied by the model parameters. Additionally, approximated lumped descriptions, representing the tyre dynamics using simpler systems of ODEs, are derived starting from the distributed formulations. Finally, Sect. 5 summarises the main findings of the paper, and outlines future directions for research.

2   Theories of transient tyre dynamics

The present section introduces the two formulations that are dealt with in this paper: the classic and the LuGre-brush models.

2.1   The brush model

In the brush models, the rolling contact between the tyre and the road takes place inside a small area, called contact patch, and denoted here with $\mathscr{P}$. In this paper, it is assumed that $\mathscr{P} = \{\xi \in \mathbb{R} \mid 0 \leq \xi \leq 2a\}$ is a compact, convex subset of $\mathbb{R}$. Moreover, $\mathscr{P}$ is also supposed to be fixed in time or, equivalently, over travelled distance. In particular, assuming that the rolling speed of the tyre satisfies $V_{\mathrm{r}}(s) > 0$, when the camber angle and the turning spin are sufficiently small [1, 75, 76], the governing PDEs of the brush model may be formulated as follows using the travelled distance $s \triangleq \int_0^t V_{\mathrm{r}}(t')\,\mathrm{d}t'$ as independent variable:

$$\bar{\boldsymbol{v}}_{\mathrm{s}}(\xi, s) = -\boldsymbol{\sigma}'(s) - \mathbf{A}_\varphi(s) \begin{bmatrix} a - \xi \\ 0 \end{bmatrix} + \frac{\partial \boldsymbol{u_t}(\xi, s)}{\partial s} + \frac{\partial \boldsymbol{u_t}(\xi, s)}{\partial \xi}, \qquad (\xi, s) \in \mathring{\mathscr{P}} \times \mathbb{R}_{>0}. \tag{1}$$

In Eq. (1), $\bar{\boldsymbol{v}}_{\mathrm{s}}(\xi, s) = [\bar{v}_{\mathrm{s}x}(\xi, s)\ \bar{v}_{\mathrm{s}y}(\xi, s)]^{\mathrm{T}}$ represents the so-called *micro-sliding velocity*, $\boldsymbol{u_t}(\xi, s) = [u_x(\xi, s)\ u_y(\xi, s)]^{\mathrm{T}}$ is the tangential displacement of the bristle inside the contact patch $\mathscr{P}$, the vector $\boldsymbol{\sigma}'(s) = [\sigma'_x(s)\ \sigma'_y(s)]^{\mathrm{T}} \triangleq -\boldsymbol{V}'_{\mathrm{s}}(s)/V_{\mathrm{r}}(s)$ denotes the transient translational slip, $\boldsymbol{V}'_{\mathrm{s}}(s) = [V'_{\mathrm{s}x}(s)\ V'_{\mathrm{s}y}(s)]^{\mathrm{T}}$ represents the transient sliding velocity, and $\mathbf{A}_\varphi(s)$ is the spin tensor, defined as [76]

$$\mathbf{A}_\varphi(s) = \begin{bmatrix} 0 & -\varphi(s) \\ \varphi(s) & 0 \end{bmatrix}, \tag{2}$$

being $\varphi(s)$ is the spin variable. In turn, the transient slip $\boldsymbol{\sigma}'(s)$ may be expressed as a function of the rigid translational slip $\boldsymbol{\sigma}(s) = [\sigma_x(s)\ \sigma_y(s)]^{\mathrm{T}} \triangleq -\boldsymbol{V}_{\mathrm{s}}(s)/V_{\mathrm{r}}(s)$ (where $\boldsymbol{V}_{\mathrm{s}}(s) = [V_{\mathrm{s}x}(s)\ V_{\mathrm{s}y}(s)]^{\mathrm{T}}$ denotes the sliding velocity) and the tangential deformation of the tyre carcass $\boldsymbol{\delta_t}(s) = [\delta_x(s)\ \delta_y(s)]^{\mathrm{T}}$:

$$\boldsymbol{\sigma}'(s) = \boldsymbol{\sigma}(s) - \frac{\mathrm{d}\boldsymbol{\delta_t}(s)}{\mathrm{d}s}. \tag{3}$$

It is worth observing the relationship $\boldsymbol{V}'_{\mathrm{s}}(s) = \boldsymbol{V}_{\mathrm{s}}(s) + \dot{\boldsymbol{\delta}}(s)$ between the transient sliding velocity and the coventional one. The situation is illustrated schematically in Fig. 1.

The above PDEs (1) also come equipped with a boundary (BC) and initial condition (IC):

BC: $\qquad \boldsymbol{u_t}(0, s) = \boldsymbol{0}, \qquad\qquad s \in \mathbb{R}_{>0}, \tag{4a}$

IC: $\qquad \boldsymbol{u_t}(\xi, 0) = \boldsymbol{u_{t0}}(\xi), \qquad\qquad \xi \in \mathring{\mathscr{P}}, \tag{4b}$

ideally with $\boldsymbol{u_{t0}} \in C^1(\mathring{\mathscr{P}}; \mathbb{R}^2)$, and the IC satisfying the so-called *compatibility condition* $\boldsymbol{u_{t0}}(0) = \boldsymbol{0}$. Physically, the compatibility condition is motivated by frictional considerations. In this paper, ICs of the type $\boldsymbol{u_{t0}} \in C^0(\mathring{\mathscr{P}})$ are more generally considered, but the compatibility condition is always supposed to be fulfilled.

Equation (1) is moreover accompanied by two algebraic conditions, which differentiate between the local stick and slip behaviour, according to the simplest Amontons-Coulomb friction friction model:

$$\bar{\boldsymbol{v}}_{\mathrm{s}}(\xi, s) = \boldsymbol{0} \implies q_{\boldsymbol{t}}(\xi, s) \leq \mu q_z(\xi), \tag{5a}$$
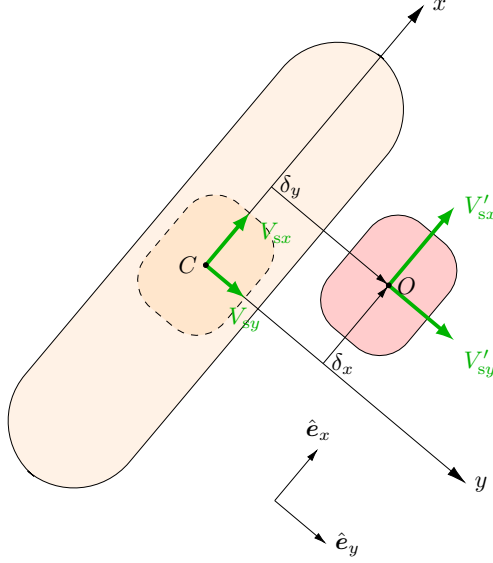
3

Figure 1: Schematic illustration of the tyre with a flexible carcass. The centre of the contact patch in the undeformed configuration is denoted by C and travels with sliding velocity $\boldsymbol{V}_\mathrm{s}(s)$. After the displacement of the tyre carcass, the centre moves to point O and travels with transient sliding velocity $\boldsymbol{V}'_\mathrm{s}(s) = \boldsymbol{V}_\mathrm{s}(s) + \dot{\boldsymbol{\delta}}(s)$. Note that, in this paper, the lateral dimension of the contact patch is neglected.

$$\bar{\boldsymbol{v}}_\mathrm{s}(\xi, s) \neq \boldsymbol{0} \iff \boldsymbol{q_t}(\xi, s) = \mu q_z(\xi)\hat{\boldsymbol{s}_t}(\xi, s), \tag{5b}$$

where the *sliding direction* $\hat{\boldsymbol{s}_t}(\xi, s)$ is defined as

$$\hat{\boldsymbol{s}_t}(\xi, s) \triangleq -\frac{\bar{\boldsymbol{v}}_\mathrm{s}(\xi, s)}{\bar{v}_\mathrm{s}(\xi, s)}. \tag{6}$$

In Eqs. (5) and (6), $\bar{v}_\mathrm{s}(\xi, s) = \left\|\bar{\boldsymbol{v}}_\mathrm{s}(\xi, s)\right\|$ denotes the total mico-sliding velocity, $q_t(\xi, s) = \left\|\boldsymbol{q_t}(\xi, s)\right\|$, with $\boldsymbol{q_t}(\xi, s) = [q_x(\xi, s) \ q_y(\xi, s)]^\mathrm{T}$, represents the total tangential stress acting locally upon the bristles, $q_z(\xi)$ is the vertical pressure distribution, and μ is the friction coefficient. Generally speaking, the latter may exhibit strong dependencies upon other local quantities, such as temperature and position inside the contact patch [64, 65, 68–70, 72]. However, for the sake of simplicity, this paper restricts to consider a constant value for the friction coefficient when dealing with the standard version of the brush models[1].

The interpretation of Eq. (5a) is basically as follows: a bristle travelling inside the contact patch adheres to the ground only if the magnitude of the shear stress acting upon it is lower than the product $\mu q_z(\xi)$, traditionally referred to as *traction bound*. When the shear stress exceeds the available friction, the bristle starts sliding and the nondimensional micro-sliding velocity suddenly increases, i.e., $\bar{v}_\mathrm{s}(\xi, s) > 0$. In view of these considerations, the contact patch may be partitioned into an adhesion region $\mathscr{P}^{(\mathrm{a})}$ and a sliding one $\mathscr{P}^{(\mathrm{s})}$ defined by

$$\mathscr{P}^{(\mathrm{a})} \triangleq \left\{\xi \in \mathscr{P} \mid \text{Eq. (5a) holds}\right\}, \tag{7a}$$

$$\mathscr{P}^{(\mathrm{s})} \triangleq \left\{\xi \in \mathscr{P} \mid \text{Eq. (5b) holds}\right\}. \tag{7b}$$

The closure relationships to Eqs. (1), (5) and (6) are finally provided by the constitutive and equilibrium equations. The first set of equations relates the shear stresses $\boldsymbol{q_t}(\xi, s) = [q_x(\xi, s) \ q_y(\xi, s)]^\mathrm{T}$ acting at the contact patch to the deformation of the bristles, and the global tyre forces to the deflection of the tyre carcass, respectively. In particular, concerning the bristle displacement, a local linear constitutive relationship is traditionally postulated:

$$\boldsymbol{q_t}(\xi, s) = \mathbf{K_t}\boldsymbol{u_t}(\xi, s), \tag{8}$$

---

[1]It may be understood that the assumption of constant friction coefficient ensures the initial conditions to be at least $C^0(\mathring{\mathscr{P}}_0)$.

4

where the operator $\mathbf{K_t} \in \mathbb{R}^{2 \times 2}$ represents a diagonal matrix[2], i.e.,

$$\mathbf{K_t} = \begin{bmatrix} k_{xx} & k_{xy} \\ k_{yx} & k_{yy} \end{bmatrix} = \begin{bmatrix} k_x & 0 \\ 0 & k_y \end{bmatrix}. \tag{9}$$

Similarly, the tyre carcass is assumed to behave as a linear translational spring, according to

$$\boldsymbol{F_t}(s) = \mathbf{C}' \boldsymbol{\delta_t}(s), \tag{10}$$

being $\mathbf{C}' \in \mathbb{R}^{2 \times 2}$ a diagonal matrix of the type

$$\mathbf{C}' = \begin{bmatrix} C'_{xx} & C'_{xy} \\ C'_{yx} & C'_{yy} \end{bmatrix} = \begin{bmatrix} C'_x & 0 \\ 0 & C'_y \end{bmatrix}. \tag{11}$$

Its inverse is denoted in this paper by $\mathbf{S}' \triangleq \mathbf{C}'^{-1}$:

$$\mathbf{S}' = \begin{bmatrix} S'_{xx} & S'_{xy} \\ S'_{yx} & S'_{yy} \end{bmatrix} = \begin{bmatrix} S'_x & 0 \\ 0 & S'_y \end{bmatrix} \equiv \begin{bmatrix} \dfrac{1}{C'_x} & 0 \\ 0 & \dfrac{1}{C'_y} \end{bmatrix}. \tag{12}$$

Lastly, the equilibrium equations allow expressing the tyre forces $\boldsymbol{F_t}(s) = [F_x(s)\ F_y(s)]^{\mathrm{T}}$ and moment $M_z(s)$ as integral functions of the tangential shear stresses. Integrating the shear stresses over the contact patch provides the following formulae:

$$\boldsymbol{F_t}(s) = \int_{\mathscr{P}} \boldsymbol{q_t}(\xi, s)\, \mathrm{d}\xi, \tag{13a}$$

$$M_z(s) = \int_{\mathscr{P}} (2a - \xi) q_y(\xi, s)\, \mathrm{d}\xi. \tag{13b}$$

2.2 The LuGre-brush model

The LuGre-brush formulation, developed originally by Deur [35–38] and Velenis and Tsiotras [39–41], qualifies as a control-oriented model, and builds upon the friction theory proposed by Canudas-de-Wit and Åström in their seminal paper [47]. In the LuGre variant of the brush models, the main variable is represented by an internal frictional state $\boldsymbol{z}(\xi, s) = [z_x(\xi, s)\ z_y(\xi, s)]^{\mathrm{T}}$, which may eventually be interpreted as the deformation of a bristle travelling inside the contact patch. Accordingly, the governing PDEs of the model replicate the structure of Eqs. (1), but introduce an additional damping term, often referred to as *dissipative term*, that accounts for pre-sliding and Stribeck-induced effects. When considering a dynamic tyre carcass, the governing equations of the LuGre-brush model may be formulated as follows:

$$\frac{\partial \boldsymbol{z}(\xi, s)}{\partial s} + \frac{\partial \boldsymbol{z}(\xi, s)}{\partial \xi} = \boldsymbol{\sigma}'(s) + \mathbf{A}_\varphi(s) \begin{bmatrix} a - \xi \\ 0 \end{bmatrix} - \frac{\hat{v}_\mu(s)}{V_{\mathrm{r}}(s) g(\hat{v}_\mu(s))} \mathbf{C}_0 \boldsymbol{z}(\xi, s), \quad (\xi, s) \in \mathring{\mathscr{P}} \times \mathbb{R}_{>0}, \tag{14}$$

where $V_{\mathrm{r}}(s) > 0$ is the rolling velocity of the tyre, the term $\hat{v}_\mu(s) = \|\hat{\boldsymbol{v}}_\mu(s)\|$, with $\hat{\boldsymbol{v}}_\mu(s) = [\hat{v}_{\mu x}(s)\ \hat{v}_{\mu y}(s)]^{\mathrm{T}}$, is an approximated expression for the total sliding velocity of the tyre, usually averaged over the contact patch and assumed to be dependent only upon the rolling velocity and on the slip inputs [38], and the matrix

$$\mathbf{C}_0 = \begin{bmatrix} c_{0xx} & c_{0xy} \\ c_{0yx} & c_{0yy} \end{bmatrix} = \begin{bmatrix} c_{0x} & 0 \\ 0 & c_{0y} \end{bmatrix} \tag{15}$$

is a diagonal matrix, whose entries have the dimension of a curvature. The spin tensor $\mathbf{A}_\varphi(s)$ and the transient slip vector $\boldsymbol{\sigma}'(s)$ appearing in Eq. (14) are defined as for the standard variant of the brush models, i.e., according to Eqs. (2) and (3), respectively. Finally, the *sliding function* $g(\cdot)$ is a monothonically decreasing function of its argument, usually postulated in the form

$$g(\hat{v}_\mu(s)) = \mu_{\mathrm{d}} + (\mu_{\mathrm{s}} - \mu_{\mathrm{d}}) \mathrm{e}^{-(\hat{v}_\mu(s)/v_\delta)^\delta}, \tag{16}$$

---

[2]In this paper, the mathematical exposition is carried out under the assumption of diagonal matrices, also for the LuGre-brush model. This is done not only to lighten the equations and the proofs in Appendices A.1 and A.2, but also because in practice the assumption is actually standard, and there is generally no need to account for cross elements. However, most of the proofs and results presented in the paper may be extended in a straightforwad way to account for nondiagonal matrices.

where $\mu_{\rm s}$ and $\mu_{\rm d}$ are the static and dynamic friction coefficients, with $\mu_{\rm d} \leq \mu_{\rm s}$, v_δ is the *Stribeck velocity*, and δ is the *Stribeck exponent*. It should be observed that $\mu_{\rm d}$ and $\mu_{\rm s}$ are global quantities in the LuGre friction model, meaning that they are not function of the position inside the contact patch $\mathscr{P}$.

The vector-valued transport PDE (14) comes equipped with similar BC and IC to those in Eqs. (4), that is,

$$\text{BC:} \qquad \boldsymbol{z}(0,s) = \boldsymbol{0}, \qquad\qquad s \in \mathbb{R}_{>0}, \qquad (17\text{a})$$

$$\text{IC:} \qquad \boldsymbol{z}(\xi,0) = \boldsymbol{z}_0(\xi), \qquad\qquad \xi \in \mathring{\mathscr{P}}, \qquad (17\text{b})$$

possibly with $\boldsymbol{z}_0 \in C^1(\mathring{\mathscr{P}}; \mathbb{R}^2)$ (more generally $\boldsymbol{z}_0 \in C^0(\mathring{\mathscr{P}}; \mathbb{R}^2)$ assuming weaker regularity), and the BC fulfilling again the compatibility condition $\boldsymbol{z}_0(0) = 0$.

Concerning the constitutive equations, the relationship between the tangential forces and the deflection of the tyre carcass is assumed to be linear elastic, and given again by Eq. (10). However, as opposed to the standard version of the brush models, in the LuGre formulation, the shear stresses are not determined directly from the frictional state $\boldsymbol{z}(\xi,s)$. Instead, the latter is used to calculate a *shear contribution coefficient* $\boldsymbol{\mu}(\xi,s) = [\mu_x(\xi,s) \ \mu_y(\xi,s)]^{\rm T}$ varying inside the contact patch, according to the following relationship:

$$\boldsymbol{\mu}(\xi,s) = \mathbf{C}_0 \boldsymbol{z}(\xi,s) + V_{\rm r}(s)\mathbf{C}_1 \frac{\partial \boldsymbol{z}(\xi,s)}{\partial s} + V_{\rm r}(s)\mathbf{C}_2 \left(\boldsymbol{\sigma}'(s) + \mathbf{A}_\varphi(s) \begin{bmatrix} a - \xi \\ 0 \end{bmatrix} \right), \qquad (18)$$

where $\mathbf{C}_1$, $\mathbf{C}_2 \in \mathbb{R}^{2\times 2}$ are two positive semidefinite, diagonal matrices of constant parameters:

$$\mathbf{C}_1 = \begin{bmatrix} c_{1xx} & c_{1xy} \\ c_{1yx} & c_{1yy} \end{bmatrix} = \begin{bmatrix} c_{1x} & 0 \\ 0 & c_{1y} \end{bmatrix}, \qquad \text{and} \qquad \mathbf{C}_2 = \begin{bmatrix} c_{2xx} & c_{2xy} \\ c_{2yx} & c_{2yy} \end{bmatrix} = \begin{bmatrix} c_{2x} & 0 \\ 0 & c_{2y} \end{bmatrix}. \qquad (19\text{a})$$

Their entries[3] are expressed in $\mathrm{s\,m}^{-1}$.

The tangential forces and moment exerted at the tyre-road interface are then computed by multiplying the shear contribution coefficient $\boldsymbol{\mu}(\xi,s)$ for the vertical pressure distribution $q_z(\xi)$, expressed in $\mathrm{N\,m}^{-1}$. Accordingly, integrating over the contact patch $\mathscr{P}$ yields the following expressions:

$$\boldsymbol{F_t}(s) = \int_{\mathscr{P}} \boldsymbol{\mu}(\xi,s) q_z(\xi) \,\mathrm{d}\xi, \qquad (20\text{a})$$

$$M_z(s) = \int_{\mathscr{P}} (a - \xi)\mu_y(\xi,s) q_z(\xi) \,\mathrm{d}\xi. \qquad (20\text{b})$$

Equations (20) represent the LuGre counterpart of the equilibrium equations (13).

3 Transient brush model

Whilst the transient dynamics of the tyre has traditionally been studied by resorting to more sophisticated formulations – including primarily the so-called stretched string models – the simplest variant of the brush theory still provides an adequate framework to rigorously analyse nonstationary phenomena connected with time-varying slip inputs. Therefore, the present section introduces the unsteady-state formulation of the brush models. In particular, Sect. 3.1 first recapitulates the classic results obtained neglecting the dynamics of the tyre carcass, owing to the assumption of vanishing sliding. Then, Sects. 3.2 and 3.3 extend the investigation by considering the effect of a compliant carcass under vanishing sliding conditions and for the case of limited friction, respectively.

---

[3]Concerning the LuGre-brush model, three matrices $\mathbf{C}_0$, $\mathbf{C}_1$ and $\mathbf{C}_2$ are often used. According to the original paper written by Canudas-de-Wit, Åström and Olsson, who developed the corresponding lumped formulation [47], such matrices have the meaning of stiffness, damping, and viscous friction, respectively. Since the development of the distributed formulation carried out in parallel by Deur et al. [35–38] and Velenis and Tsiotras [39–41], the units for the entries of these matrices have changed to be consistent with the definition of the shear contribution coefficient $\boldsymbol{\mu}$ according to Eq. (18). However, the interpretation is more or less the same: the first matrix $\mathbf{C}_0$ accounts for a stiffness effect, whereas $\mathbf{C}_1$ and $\mathbf{C}_2$ for damping and viscous friction phenomena.

3.1 Brush model with rigid carcass

Assuming a rigid carcass, i.e., $\boldsymbol{\sigma}'(s) \equiv \boldsymbol{\sigma}(s)$, together with vanishing sliding conditions ($\mathscr{P}^{(\mathrm{a})} \equiv \mathscr{P}$), Eq. (1) becomes

$$\frac{\partial \boldsymbol{u_t}(\xi, s)}{\partial s} + \frac{\partial \boldsymbol{u_t}(\xi, s)}{\partial \xi} = \boldsymbol{\sigma}(s) + \mathbf{A}_\varphi(s) \begin{bmatrix} a - \xi \\ 0 \end{bmatrix}, \qquad (\xi, s) \in \mathring{\mathscr{P}} \times \mathbb{R}_{>0}. \tag{21}$$

The above Eq. (21) consists of two linear, uncoupled transport PDEs involving only two partial derivatives: one taken with respect to the longitudinal coordinate ξ and one with respect to the travelled distance s.

Enforcing the BC (4a) and IC (4b), in turn, provides two different solutions to the PDE (21). These solutions are uniquely defined on $\mathscr{P}$, and may be sought using the method of the characteristic lines [80–83], which yields [34]

$$\boldsymbol{u_t^-}(\xi, s) = \int_0^\xi \boldsymbol{\sigma}\big(\xi' - \xi + s\big) + \mathbf{A}_\varphi\big(\xi' - \xi + s\big) \begin{bmatrix} a - \xi' \\ 0 \end{bmatrix} \mathrm{d}\xi', \qquad (\xi, s) \in \mathscr{P}^- \times \mathbb{R}_{\geq 0}, \tag{22a}$$

$$\boldsymbol{u_t^+}(\xi, s) = \int_0^s \boldsymbol{\sigma}\big(s'\big) + \mathbf{A}_\varphi\big(s'\big) \begin{bmatrix} a - s' + s - \xi \\ 0 \end{bmatrix} \mathrm{d}s' + \boldsymbol{u_{t0}}(\xi - s), \qquad (\xi, s) \in \mathscr{P}^+ \times \mathbb{R}_{\geq 0}. \tag{22b}$$

In Eqs. (22), the deflections $\boldsymbol{u_t^-}(\xi, s) = [u_x^-(\xi, s) \; u_y^-(\xi, s)]^\mathrm{T}$ and $\boldsymbol{u_t^+}(\xi, s) = [u_x^+(\xi, s) \; u_y^+(\xi, s)]^\mathrm{T}$ result from the application of the BC and IC in turn, respectively. The corresponding subdomains $\mathscr{P}^-$ and $\mathscr{P}^+$ of the contact patch may be defined by setting $\mathscr{P}^- \triangleq \{\xi \in \mathscr{P} \mid 0 \leq \xi < s\}$, and $\mathscr{P}^+ \triangleq \{\xi \in \mathscr{P} \mid s \leq \xi \leq 2a\}$. Accordingly, the global solution $\boldsymbol{u_t}(\xi, s)$ over $\mathscr{P}$ may then be constructed as

$$\boldsymbol{u_t}(\xi, s) = \begin{cases} \boldsymbol{u_t^-}(\xi, s), & (\boldsymbol{\xi}, s) \in \mathscr{P}^- \times \mathbb{R}_{\geq 0}, \\ \boldsymbol{u_t^+}(\xi, s), & (\boldsymbol{\xi}, s) \in \mathscr{P}^+ \times \mathbb{R}_{\geq 0}, \end{cases} \tag{23}$$

since $\mathscr{P} = \mathscr{P}^- \cup \mathscr{P}^+$. It may be easily observed that, owing to the compatibility assumption, $\boldsymbol{u_t} \in C^0(\mathscr{P} \times \mathbb{R}_{\geq 0}; \mathbb{R}^2)$, the deflections $\boldsymbol{u_t^-}(\xi, s)$ and $\boldsymbol{u_t^+}(\xi, s)$ are continuous for $\xi = s$, i.e., $\boldsymbol{u_t^-}(s, s) \equiv \boldsymbol{u_t^+}(s, s)$. Unfortunately, the continuity at $\xi = s$ is the only requirement that the global solution may be expected to fulfil. This consideration holds also true for the solution $\boldsymbol{u_t^+}(\xi, s)$, which is often only $C^0(\mathscr{P}^+ \times \mathbb{R}_{\geq 0}; \mathbb{R}^2)$, unless $\boldsymbol{u_{t0}} \in C^1(\mathscr{P}; \mathbb{R}^2)$. Actually, this only happens if the initial condition itself corresponds to a distribution which results already from a stationary configuration in vanishing sliding conditions[4].

This aspect is perhaps better understood by observing that the expressions $\boldsymbol{u_t^-}(\xi, s)$ and $\boldsymbol{u_t^+}(\xi, s)$ in Eqs. (22) may be interpreted as the stationary and the transient solutions to the PDEs (21), respectively. Indeed, it may be easily inferred from the definition of $\mathscr{P}^-$ and $\mathscr{P}^+$ that the transient extinguishes after a value of the travelled distance equal to $s = 2a$, where $2a$ is the maximum length of the contact patch. After that the tyre has travelled a distance equal to $s = 2a$, the solution $\boldsymbol{u_t^-}(\xi, s)$ extends all over $\mathscr{P}$. It is, however, still time-varying, and depends upon the specific expressions of the translational slip and spin parameters. The observations above may be formalised mathematically considering the notion of input-to-state stability, which has been recently extended to systems of PDEs and interconnected PDE-ODEs [84]. In this paper, the notion of input-to-state stability is mainly used to highlight some essential aspects connected to the presence (or absence) of a dynamic tyre carcass model. More specifically, departing from the closed-form solutions in Eqs. (22), the following estimates may be derived, as asserted by Proposition 3.1.

Proposition 3.1. *Equations* (22) *satisfy the following input-to-state stability estimates:*

$$\big\|u_x(\cdot, s)\big\|_\infty \leq \big\|u_{x0}(\cdot)\big\|_\infty \mathrm{e}^{-\rho(s-2a)} + \max_{s' \in [0,s]} 2a\big|\sigma_x\big(s'\big)\big|, \quad s \in \mathbb{R}_{\geq 0}, \tag{24a}$$

$$\big\|u_y(\cdot, s)\big\|_\infty \leq \big\|u_{y0}(\cdot)\big\|_\infty \mathrm{e}^{-\rho(s-2a)} + \max_{s' \in [0,s]} \left(2a\big|\sigma_y\big(s'\big)\big| + \frac{a^2}{2}\big|\varphi\big(s'\big)\big|\right), \quad s \in \mathbb{R}_{\geq 0}, \tag{24b}$$

for some $\rho \in \mathbb{R}_{>0}$.

Proof. See Appendix A.1 $\qquad\qquad\square$

---

[4]Therefore, the transient brush theory may be seen as a *weak* one, in the sense that the solutions are always $C^0(\mathscr{P} \times \mathbb{R}_{\geq 0}; \mathbb{R}^2)$, but higher regularity cannot be required.

The interpretation of the inequalities (24) is rather straightforward: the longitudinal and lateral components of the maximum deflection of the bristles are upper-bounded by an exponentially-decreasing term involving the initial conditions, plus an additional contribution that relates to the slip inputs. This is in agreement with what discussed previously, since the initial conditions are completely shoved out from the contact patch after travelling a distance equal to the contact length.

3.2 Brush model with flexible carcass (linear full contact patch)

When considering the compliance of the tyre carcass under vanishing sliding conditions, the conventional translational slip variables $\boldsymbol{\sigma}(s)$ in Eq. (21) may be replaced by the transient slip $\boldsymbol{\sigma}'(s)$, yielding

$$\frac{\partial \boldsymbol{u_t}(\xi,s)}{\partial s} + \frac{\partial \boldsymbol{u_t}(\xi,s)}{\partial \xi} = \boldsymbol{\sigma}'(s) + \mathbf{A}_\varphi(s) \begin{bmatrix} a - \xi \\ 0 \end{bmatrix}, \qquad (\xi,s) \in \mathring{\mathscr{P}} \times (0,S). \tag{25}$$

The resulting problem is rather involved compared to that described by Eq. (21), since the transient slip $\boldsymbol{\sigma}'(s)$ depends upon the deformation of the bristles through integration over the contact patch. In fact, it may be recast more conveniently as

$$\boldsymbol{\sigma}'(s) = \boldsymbol{\sigma}(s) - \frac{\mathrm{d}\boldsymbol{\delta_t}(s)}{\mathrm{d}s} = \boldsymbol{\sigma}(s) - \mathbf{S}'\mathbf{K_t} \int_{\mathscr{P}} \frac{\partial \boldsymbol{u_t}(\xi,s)}{\partial s}\, \mathrm{d}\xi. \tag{26}$$

Combining Eq. (1) together with (26) and integrating by parts yields, after some manipulations [34],

$$\boldsymbol{\sigma}'(s) = \big(\mathbf{I} + 2a\mathbf{S}'\mathbf{K_t}\big)^{-1}\big[\boldsymbol{\sigma}(s) + \mathbf{S}'\mathbf{K_t}\boldsymbol{u_t}(2a,s)\big]. \tag{27}$$

Inserting Eq. (41) into (1) finally gives

$$\frac{\partial \boldsymbol{u_t}(\xi,s)}{\partial s} + \frac{\partial \boldsymbol{u_t}(\xi,s)}{\partial \xi} = \big(\mathbf{I} + 2a\mathbf{S}'\mathbf{K_t}\big)^{-1}\big[\boldsymbol{\sigma}(s) + \mathbf{S}'\mathbf{K_t}\boldsymbol{u_t}(2a,s)\big] + \tilde{\mathbf{I}} \begin{bmatrix} a - \xi \\ 0 \end{bmatrix} \varphi(s), \quad (\xi,s) \in \mathring{\mathscr{P}} \times (0,S), \tag{28}$$

where

$$\tilde{\mathbf{I}} \triangleq \begin{bmatrix} 0 & -1 \\ 1 & 0 \end{bmatrix}. \tag{29}$$

Equation (39) allows expressing the transient deflection of the bristles as a function of the original slip and spin variables $(\boldsymbol{\sigma}, \varphi)$, and the boundary term (trace term) $\boldsymbol{u_t}(2a,s)$ at the trailing edge. In this paper, the formulation derived above is renamed *linear full contact patch*.

3.2.1 Analytical solution

Concerning the classic formulation of the brush models with flexible carcass, the first result derived in this paper consists of the following Theorem 3.1. The proof is similar to those of Theorems 2.6 and 9.1 in [84], altough with minor differences, and is detailed in Appendix A.1.

Theorem 3.1 (Existence and uniqueness of the solution for the linear full contact patch model)**.** *Under the assumption $(\boldsymbol{\sigma}, \varphi) \in C^0([0,S]; \mathbb{R}^3)$ and $\boldsymbol{u_{t0}} \in C^0(\mathscr{P}; \mathbb{R}^2)$, Eq. (25) equipped with BC and IC (4a) and (4b) admits a unique solution $C^0(\mathscr{P} \times [0,S]; \mathbb{R}^2)$ in the form of Eq. (23), with $\boldsymbol{u_t^-}(\xi,s)$ and $\boldsymbol{u_t^+}(\xi,s)$ satisfying*

$$\boldsymbol{u_t^-}(\xi,s) = \int_0^\xi \big(\mathbf{I} + 2a\mathbf{S}'\mathbf{K_t}\big)^{-1}\mathbf{S}'\mathbf{K_t}\boldsymbol{u_t}\big(2a, \xi' - \xi + s\big)\, \mathrm{d}\xi' + \int_0^\xi \big(\mathbf{I} + 2a\mathbf{S}'\mathbf{K_t}\big)^{-1}\boldsymbol{\sigma}\big(\xi' - \xi + s\big)\, \mathrm{d}\xi'$$
$$+ \int_0^\xi \tilde{\mathbf{I}} \begin{bmatrix} a - \xi' \\ 0 \end{bmatrix} \varphi\big(\xi' - \xi + s\big)\, \mathrm{d}\xi', \quad (\xi,s) \in \mathscr{P}^- \times [0,S], \tag{30a}$$

$$\boldsymbol{u_t^+}(\xi,s) = \int_0^s \big(\mathbf{I} + 2a\mathbf{S}'\mathbf{K_t}\big)^{-1}\mathbf{S}'\mathbf{K_t}\boldsymbol{u_t}\big(2a, s'\big)\, \mathrm{d}s' + \int_0^s \big(\mathbf{I} + 2a\mathbf{S}'\mathbf{K_t}\big)^{-1}\boldsymbol{\sigma}\big(s'\big)\, \mathrm{d}s'$$
$$+ \int_0^s \tilde{\mathbf{I}} \begin{bmatrix} a - s' + s - \xi \\ 0 \end{bmatrix} \varphi\big(s'\big)\, \mathrm{d}s' + \boldsymbol{u_{t0}}(\xi - s), \quad (\xi,s) \in \mathscr{P}^+ \times [0,S]. \tag{30b}$$

Proof. See Appendix A.1 □

In vanishing sliding conditions, Theorem 3.1 asserts the existence and the uniqueness of a weak or generalised solution to the governing PDEs of the brush models with flexible carcass. At first glance, the result appears to be merely qualitative in nature, since the solution derived in Eq. (30) is still expressed in integral form, and is therefore implicit. In reality, an analytical formula for the trace term $\boldsymbol{u_t}(2a, \cdot)$ appearing in Eqs. (30) may be sought amongst the functions satisfying the following delay differential equations (DDEs):

$$\frac{\partial \boldsymbol{u_t}(2a, s)}{\partial s} = \left(\mathbf{I} + 2a\mathbf{S'}\mathbf{K_t}\right)^{-1}\mathbf{S'}\mathbf{K_t}\boldsymbol{u_t}(2a, s) + \left(\mathbf{I} + 2a\mathbf{S'}\mathbf{K_t}\right)^{-1}\boldsymbol{\sigma}(s)$$
$$- \tilde{\mathbf{I}}\begin{bmatrix} a \\ 0 \end{bmatrix}\varphi(s) + \int_0^s \tilde{\mathbf{I}}\begin{bmatrix} 1 \\ 0 \end{bmatrix}\varphi(s')\,\mathrm{d}s' + \frac{\partial \boldsymbol{u_{t0}}(2a - s)}{\partial s}, \quad s \in [0, 2a), \tag{31}$$

and

$$\frac{\partial \boldsymbol{u_t}(2a, s)}{\partial s} = \left(\mathbf{I} + 2a\mathbf{S'}\mathbf{K_t}\right)^{-1}\mathbf{S'}\mathbf{K_t}\left[\boldsymbol{u_t}(2a, s) - \boldsymbol{u_t}(2a, s - 2a)\right] + \left(\mathbf{I} + 2a\mathbf{S'}\mathbf{K_t}\right)^{-1}\left[\boldsymbol{\sigma}(s) - \boldsymbol{\sigma}(s - 2a)\right]$$
$$- \tilde{\mathbf{I}}\begin{bmatrix} a \\ 0 \end{bmatrix}\left[\varphi(s) + \varphi(s - 2a)\right] + \int_0^{2a} \tilde{\mathbf{I}}\begin{bmatrix} 1 \\ 0 \end{bmatrix}\varphi(\xi' - 2a + s)\,\mathrm{d}\xi', \quad s \in [2a, S], \tag{32}$$

It is worth mentioning that the solutions of Eq. (30) may not solve (31) and (31), since these generally require higher regularity. However, after some straightforward but tedious manipulations, the solutions to the above Eqs. (31) and (32) may be recovered explicitly as

$$\boldsymbol{u_t}(2a, s) = \boldsymbol{u_{t0}}(2a - s) + \int_0^s \boldsymbol{\Phi_{\sigma'}}\left(s, s'\right)\left[\left(\mathbf{I} + 2a\mathbf{S'}\mathbf{K_t}\right)^{-1}\boldsymbol{\sigma}\left(s'\right) - \tilde{\mathbf{I}}\begin{bmatrix} a \\ 0 \end{bmatrix}\varphi\left(s'\right)\right]\mathrm{d}s'$$
$$+ \int_0^s \boldsymbol{\Phi_{\sigma'}}\left(s, s'\right)\int_0^{s'} \tilde{\mathbf{I}}\begin{bmatrix} 1 \\ 0 \end{bmatrix}\varphi(\tilde{s})\,\mathrm{d}\tilde{s}\,\mathrm{d}s' - \int_0^s \frac{\partial \boldsymbol{\Phi_{\sigma'}}\left(s, s'\right)}{\partial s'}\boldsymbol{u_{t0}}\left(2a - s'\right)\mathrm{d}s', \quad s \in [0, 2a), \tag{33}$$

and

$$\boldsymbol{u_t}(2a, s) = \boldsymbol{\Phi_{\sigma'}}\left(s, 2na\right)\boldsymbol{u_t}(2a, 2na) - \int_{2na}^s \boldsymbol{\Phi_{\sigma'}}\left(s, s'\right)\left(\mathbf{I} + 2a\mathbf{S'}\mathbf{K_t}\right)^{-1}\mathbf{S'}\mathbf{K_t}\boldsymbol{u_t}\left(2a, s' - 2a\right)\mathrm{d}s'$$
$$+ \int_{2na}^s \boldsymbol{\Phi_{\sigma'}}\left(s, s'\right)\left(\mathbf{I} + 2a\mathbf{S'}\mathbf{K_t}\right)^{-1}\left[\boldsymbol{\sigma}\left(s'\right) - \boldsymbol{\sigma}\left(s' - 2a\right)\right]\mathrm{d}s'$$
$$- \int_{2na}^s \boldsymbol{\Phi_{\sigma'}}\left(s, s'\right)\tilde{\mathbf{I}}\begin{bmatrix} a \\ 0 \end{bmatrix}\left[\varphi\left(s'\right) + \varphi\left(s' - 2a\right)\right]\mathrm{d}s'$$
$$+ \int_{2na}^s \boldsymbol{\Phi_{\sigma'}}\left(s, s'\right)\int_0^{2a} \tilde{\mathbf{I}}\begin{bmatrix} 1 \\ 0 \end{bmatrix}\varphi\left(\xi' - 2a + s'\right)\mathrm{d}\xi'\,\mathrm{d}s', \quad s \in [2na, 2(n + 1)a), \tag{34}$$

for $n \in \mathbb{N}$. The *transient slip* transition matrix appearing in Eqs. (33) and (34) reads

$$\boldsymbol{\Phi_{\sigma'}}(s, \tilde{s}) = \mathrm{e}^{\left(\mathbf{I} + 2a\mathbf{S'}\mathbf{K_t}\right)^{-1}\mathbf{S'}\mathbf{K_t}(s - \tilde{s})}. \tag{35}$$

The explicit solution to the problem under consideration, consisting of Eqs. (30), (33) and (34), appears to be novel. It is worth noticing that, as opposed to (31) and (32), Eqs. (33) and (34) do not involve any partial derivative with respect to the slip inputs and initial conditions, and therefore are well defined even if these are only continuous functions of the travelled distance s.

In this context, Fig. 2 illustrates qualitatively the transient evolution of the longitudinal and lateral shear stresses, plotted versus the nondimensional coordinate $\bar{\xi} = \xi/(2a)$, for a tyre subjected to pure translational slip inputs $\sigma_x = \sigma_y = 0.3$, starting from an inital undeformed configuration $\boldsymbol{u_{t0}}(\xi) = \mathbf{0}$, and for different values of the nondimensional travelled distance $\bar{s} = s/(2a)$. In Fig. 2, the analytical solution (solid line) is also compared to a numerical approximation obtained using Euler's forward scheme. In particular, it may be noticed that, whilst the numerical solution appears to be sufficiently smooth even for $\bar{s} < 1$, the analytical one is only continuous with the longitudinal coordinate. This is in line with the results previously obtained in Sect. 3.1, and may be explained recalling that, according to Eqs. (30), two different expressions for the bristle deflection are valid in the stationary and transient regions of the contact patch $\mathscr{P}^-$ and $\mathscr{P}^+$, respectively. However, as opposed to the case of rigid tyre carcass, the
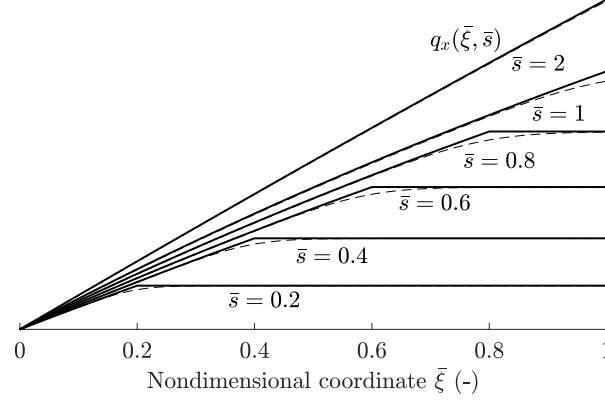
(a) $\sigma_x = 0.07$.
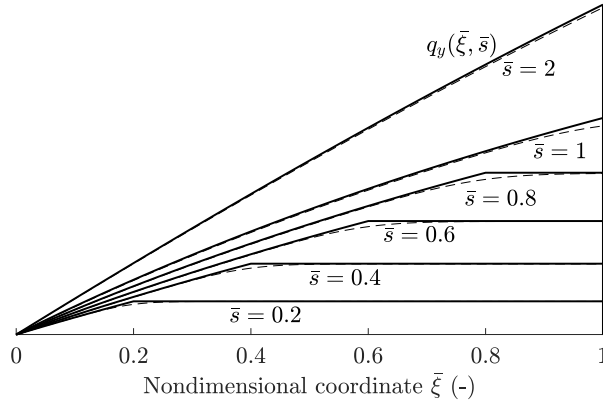
(b) $\sigma_y = 0.07$.

Figure 2: Transient evolution of the shear stresses for pure longitudinal and lateral slip inputs, for different values of the nondimensional travelled distance $\bar{s} = s/(2a)$. The solid and dashed lines refer to the analytical and numerical solutions, respectively. Tyre parameters: $k_x = k_y = k = 2.67 \cdot 10^6$ N m^{-2}, $C'_x = 6 \cdot 10^5$, $C'_y = 2.4 \cdot 10^5$ N m^{-1}, $a = 0.075$ m.

transient does not extinguish immediately after travelling a distance equal to the contact length. Indeed, the shear stresses increase relatively slower compared to the case of a rigid carcass, mainly due to the fact that the dynamics of the trace term $\boldsymbol{u_t}(2a, s)$ obeys a set of DDEs. In fact, with the values used to generate Fig. 2, steady-state conditions are reached after travelling approximately twice and thrice the contact length for the longitudinal and lateral cases, respectively (whereas, for the brush models with rigid carcass, steady-state conditions take place immediately after travelling a distance equal to the contact length). This phenomenon is traditionally referred to as *relaxation behaviour* of the tyre. In general, dynamic effects related to the compliance of the carcass are predominant over those of the bristles, especially in conjunction with instantaneous variations in the lateral slip input. However, there are several situations in which the transient deformation of the tyre tread should not be neglected [2]. The qualitative behaviour is anyway similar to that obtained when disregarding the compliance of the tyre carcass, as confirmed by the comparison with previous results advocated, e.g., in [34, 76]. Additionally, Fig. 2 shows that the dynamics of the tyre in the longitudinal direction is faster than that in the lateral one: this should be ascribed to the fact that the carcass is generally much stiffer longitudinally.

For completeness, the effect of small spin slips $\varphi = \pm 0.07$ m^{-1} upon the transient generation of the lateral shear stresses is instead depicted in Fig. 3. Also in this case, the conclusions that may be drawn are analogous to those already discussed when considering a pure translational slip input.

3.2.2 Input-to-state stability

Similarly to what done for the brush model with rigid carcass in Sect. 3.1, input-to-state stability estimates may be derived directly from the integral solutions in Eqs. (30), and read specifically as in the

(a) $\sigma_y = 0.07$, $\varphi = 0.07$.

(b) $\sigma_y = 0.07$, $\varphi = -0.7$.

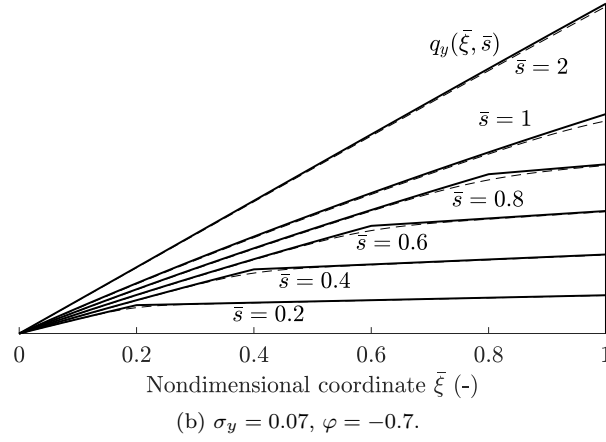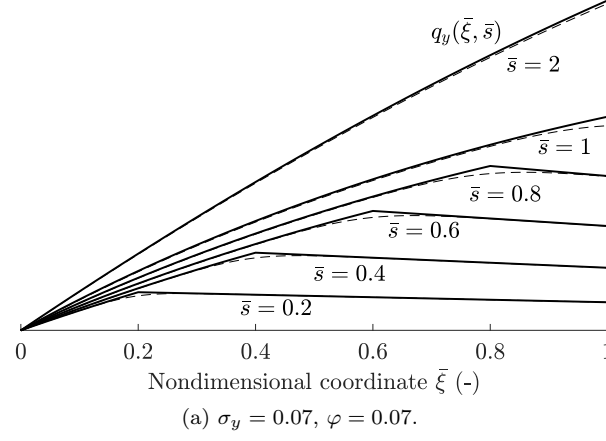Figure 3: Transient evolution of the lateral shear stresses for combined lateral slip and spin inputs, for different values of the nondimensional travelled distance $\bar{s} = s/(2a)$. The solid and dashed lines refer to the analytical and numerical solutions, respectively. Tyre parameters: $k_x = k_y = k = 2.67 \cdot 10^6$ N m^{-2}, $C'_x = 6 \cdot 10^5$, $C'_y = 2.4 \cdot 10^5$ N m^{-1}, $a = 0.075$ m.

following Lemma 3.1.

Lemma 3.1 (Input-to-state stability of the linear full contact patch model)**.** *Equations* (30) *satisfy the following input-to-state stability estimates:*

$$\big\|u_x(\cdot,s)\big\|_\infty \le \mathrm{e}^{2\rho a}\left(\frac{C_x'+2ak_x}{C_x'-2\varepsilon ak_x}\right)\big\|u_{x0}(\cdot)\big\|_\infty\,\mathrm{e}^{-\eta s} + \max_{s'\in[0,s]}\frac{2aC_x'}{C_x'-2\varepsilon ak_x}\big|\sigma_x(s')\big|,\quad s\in\mathbb{R}_{\ge0},\qquad(36\mathrm{a})$$

$$\begin{aligned}\big\|u_y(\cdot,s)\big\|_\infty &\le \mathrm{e}^{2\rho a}\left(\frac{C_y'+2ak_y}{C_y'-2\varepsilon ak_y}\right)\big\|u_{y0}(\cdot)\big\|_\infty\,\mathrm{e}^{-\eta s} + \max_{s'\in[0,s]}\frac{2aC_y'}{C_y'-2\varepsilon ak_y}\big|\sigma_y(s')\big|\\ &\quad + \max_{s'\in[0,s]}\frac{a^2}{2}\left(\frac{C_y'+2ak_y}{C_y'-2\varepsilon ak_y}\right)\big|\varphi(s')\big|,\quad s\in\mathbb{R}_{\ge0},\end{aligned}\qquad(36\mathrm{b})$$

where $\rho\in\mathbb{R}_{>0}$, *and* $\eta\in(0,\rho)$ *is a given constant for every* $\varepsilon\in\mathbb{R}_{>0}$.

Proof. See Appendix A.1 $\qquad\qquad\qquad\qquad\qquad\qquad\qquad\qquad\qquad\qquad\qquad\qquad\qquad\square$

Compared to Eqs. (24), the terms involving the initial conditions and the spin slip in the estimates (36) are amplified respectively by a factor of

$$\left(\frac{C_x'+2ak_x}{C_x'-2\varepsilon ak_x}\right)\simeq\frac{\lambda_{\sigma_x}'}{a},\qquad\qquad\text{and}\qquad\qquad\left(\frac{C_y'+2ak_y}{C_y'-2\varepsilon ak_y}\right)\simeq\frac{\lambda_{\sigma_y}'}{a},\qquad(37)$$

for an arbitrary choice of sufficiently small ε, where λ_{σ_x}' and λ_{σ_y}' denote the enhanced longitudinal and lateral relaxation lengths according to the two-regime formulation, i.e.,

$$\lambda_{\sigma_x}'\triangleq\frac{aC_x'+C_{\sigma_x}}{C_x'},\qquad\qquad\text{and}\qquad\qquad\lambda_{\sigma_x}'\triangleq\frac{aC_y'+C_{\sigma_y}}{C_y'},\qquad(38)$$

being $C_{\sigma_x}\triangleq2a^2k_x$ and $C_{\sigma_y}\triangleq2a^2k_y$ the conventional slip stiffnesses. Moreover, since $\eta\in(0,\rho)$ is strictly smaller than ρ, Eqs. (36) state that the terms involving the initial conditions decrease less rapidly than those in Eqs. (24).

In this context, the fact that the deformation of the bristles – and hence the tyre forces – might be amplified during transients is not extraneous to the two-regime tyre models, as testified by the input-to-state stability analysis conducted in [33]. The intriguing analogy between the exact formulation of the brush models with flexible carcass and the two-regime approximation seems therefore to confirm the presence of unstable dynamics (in the physical sense, since the tangential tyre forces may eventually exploit all the available friction). It should be also observed that the notion of enhanced relaxation lengths λ_{σ_x}' and λ_{σ_y}' defined as in Eq. (38) is completely absent in any other pragmatic model other than the two-regime.

3.3 Effect of limited friction (nonlinear full contact patch)

A preliminary investigation concerning the effect of limited friction may be attempted within the theoretical framework provided by the standard variant of the brush models. In this case, recalling that the nondimensional sliding velocity only vanishes in the adhesion region $\mathscr{P}^{(\mathrm{a})}$ of the contact patch, the governing PDEs of the model may be introduced in the following form:

$$\frac{\partial\boldsymbol{u}_{\boldsymbol{t}}^{(\mathrm{a})}(\xi,s)}{\partial s}+\frac{\partial\boldsymbol{u}_{\boldsymbol{t}}^{(\mathrm{a})}(\xi,s)}{\partial\xi}=\boldsymbol{\sigma}'(s)+\mathbf{A}_\varphi(s)\begin{bmatrix}a-\xi\\0\end{bmatrix},\qquad(\xi,s)\in\mathring{\mathscr{P}}^{(\mathrm{a})}\times(0,S),\qquad(39)$$

where the superscript $(\cdot)^{(\mathrm{a})}$ has been adopted to indicate that the quantities relate to the adhesion condition. The BC and IC are given again by Eqs. (4a) and (4b), respectively.

The problem described by the PDEs (39) is much more involved than the corresponding counterpart obtained under the assumption of vanishing sliding. Indeed, the presence of a time-varying sliding edge (commonly known as *breakaway point*) modifies the definition of the transient slip variable $\boldsymbol{\sigma}'(s)$ as follows:

$$\boldsymbol{\sigma}'(s)=\boldsymbol{\sigma}(s)-\frac{\mathrm{d}\boldsymbol{\delta_t}(s)}{\mathrm{d}s}=\boldsymbol{\sigma}(s)-\mathbf{S}'\mathbf{K_t}\int_{\mathscr{P}^{(\mathrm{a})}(s)}\frac{\partial\boldsymbol{u}_{\boldsymbol{t}}^{(\mathrm{a})}(\xi,s)}{\partial s}\,\mathrm{d}\xi.\qquad(40)$$

Combining Eq. (39) together with (40) and integrating by parts yields, after some manipulations [34],

$$\boldsymbol{\sigma}'(s) = \left(\mathbf{I} + \mathbf{S}'\mathbf{K_t}\xi_{\mathscr{S}}(s)\right)^{-1}\left(\boldsymbol{\sigma}(s) - \frac{1}{2}\mathbf{S}'\mathbf{K_t}\tilde{\mathbf{I}}\xi_{\mathscr{S}}(s)\begin{bmatrix}2a - \xi_{\mathscr{S}}(s)\\0\end{bmatrix}\varphi(s) + \mathbf{S}'\mathbf{K_t}\boldsymbol{u_t}\big(\xi_{\mathscr{S}}(s),s\big)\right), \qquad (41)$$

being $\xi_{\mathscr{S}}(s)$ the explicit coordinate of the sliding edge. This formulation of the problem, introduced by Guiggiani [2], is called *nonlinear full contact patch*.

The next Sects. 3.3.1 and 3.3.2 discuss qualitatively the transient behaviour of a tyre with flexible carcass when accounting for limited friction. In this context, it is essential to clarify that the derivation of the model described by Eqs. (39) and (41) builds upon some rather strong assumptions, including the existence of a unique breakaway point in transient conditions. Such condition is obviously violated for non-concave vertical pressure distributions, even in steady-state. The very nature of the underliying hypotheses, together with the technical difficulties encountered when approaching the problem in a mathematically rigorous way, substantially limit the applicability of the nonlinear full contact patch formulation, which should definitely be employed only to reveal important aspects of the nonlinear transient behaviour. Alternatively, nonstationary phenomena connected with time-varying slip inputs may be better investigated by resorting to simplified pragamatic models, such as the single contact point and the two-regime [33, 34].

3.3.1 Pure translational slip

For a step slip input $\boldsymbol{\sigma}$, the problem described by Eqs. (39) and (41) may be solved by assuming initial conditions that are oriented as the new slip value, or in isolation. Figure 4 shows the trend of the transient shear stresses $q_x(\xi, s)$ and $q_y(\xi, s)$ for the relatively high values of the longitudinal and lateral slip σ_x and $\sigma_y = 0.14$, which force the tyre to work in the nonlinear region of the steady-state characteristics. In Fig. 4, the vertical pressure distribution is assumed to follow a parabolic trend, as customarily done in the literature. Qualitatively, the transient evolution of the shear stresses is similar to that obtained analytically in Sect. 3.2 when assuming vanishing sliding conditions. However, the stresses are limited in magnitude by the traction bound $\mu q_z(\xi)$. Again, since the longitudinal and lateral slip inputs have the same value in Fig. 4 and the tyre tread is assumed to be isotropic with $k_x = k_y = k$, the steady-state distribution of shear stress coincide for both cases. On the other hand, the response to a lateral slip input is slower compared to the longitudinal case, due to the anisotropy of the tyre carcass.

It should be noticed that, in solving the transient problem, the sliding solutions may be assumed to have sign equal or opposite to the transient slips. For example, considering the pure lateral problem, the following conditions need to be satisfied:

$$u_y^{(s)}(\xi, s) = \frac{\mu}{k}q_z(\xi)\operatorname{sgn}\sigma_y'(s) \qquad \text{if} \qquad \sigma_y u_y^{(a)}\big(\xi_{\mathscr{S}}(s), s\big) \geq 0, \qquad k\left|\sigma_y'(s)\right| > \mu\frac{\partial q_z(\xi)}{\partial \xi}, \qquad (42a)$$

$$u_y^{(s)}(\xi, s) = -\frac{\mu}{k}q_z(\xi)\operatorname{sgn}\sigma_y'(s) \qquad \text{if} \qquad \sigma_y u_y^{(a)}\big(\xi_{\mathscr{S}}(s), s\big) < 0, \qquad k\left|\sigma_y'(s)\right| < -\mu\frac{\partial q_z(\xi)}{\partial \xi}, \qquad (42b)$$

Often, the last inequalities on the right-hand side of Eqs. (42) need to be checked numerically at each iteration.

3.3.2 Lateral slip and spin

Figure 5 illustrates the transient trend of the lateral shear stress in combined lateral and spin slips conditions starting from undeformed initial configurations, and assuming a parabolic pressure distribution. The two plots refer to the situations of concordant and discordant spin slip $\varphi = \pm 0.07$. In both cases, the constant lateral slip input is fixed to $\sigma_y = 0.14$. The values of the tyre parameters used to produce Fig. 5 are the same as previously. The situation is again very similar to that investigated analytically in Sect. 3.2. Moreover, the corresponding conditions of Eqs. (42) become

$$u_y^{(s)}(\xi) = \frac{\mu}{k}q_z(\xi)\operatorname{sgn}\sigma_y'(s) \quad \text{if} \quad \sigma_y'(s)u_y^{(a)}\big(\xi_{\mathscr{S}}(s), s\big) \geq 0, \quad \left|\sigma_y'(s)\right| > \Big(\varphi^{\mathrm{cr}} - |\varphi|\operatorname{sgn}\big(\sigma_y'(s)\varphi\big)\Big)(a - \xi),$$
$$(43a)$$

$$u_y^{(s)}(\xi) = -\frac{\mu}{k}q_z(\xi)\operatorname{sgn}\sigma_y'(s) \quad \text{if} \quad \sigma_y'(s)u_y^{(a)}\big(\xi_{\mathscr{S}}(s), s\big) < 0, \quad \left|\sigma_y'(s)\right| < \Big(\varphi^{\mathrm{cr}} + |\varphi|\operatorname{sgn}\big(\sigma_y'(s)\varphi\big)\Big)(\xi - a),$$
$$(43b)$$

and need to be checked iteratively.

(a) $\sigma_x = 0.14$.

(b) $\sigma_y = 0.14$.

Figure 4: Transient evolution of the shear stresses for pure longitudinal and lateral slip inputs with limited friction, for different values of the nondimensional travelled distance $\bar{s} = s/(2a)$. The solid and dashed lines refer to the analytical and numerical solutions, respectively. Tyre parameters: $F_z = 3000$ N, $k_x = k_y = k = 2.67 \cdot 10^6$ N m^{-2}, $C'_x = 6 \cdot 10^5$, $C'_y = 2.4 \cdot 10^5$ N m^{-1}, $a = 0.075$ m, $\mu = 1$.

(a) $\sigma_y = 0.14$, $\varphi = 0.07$.

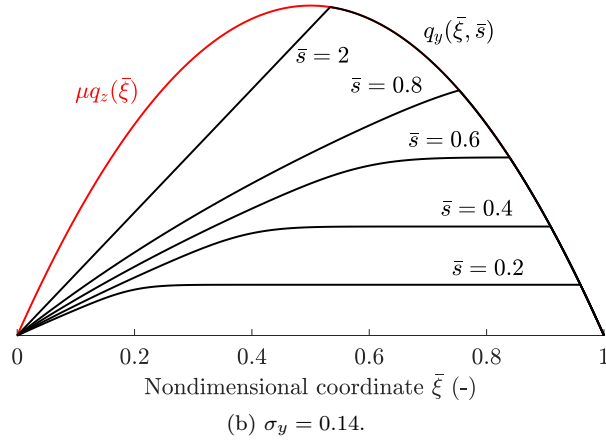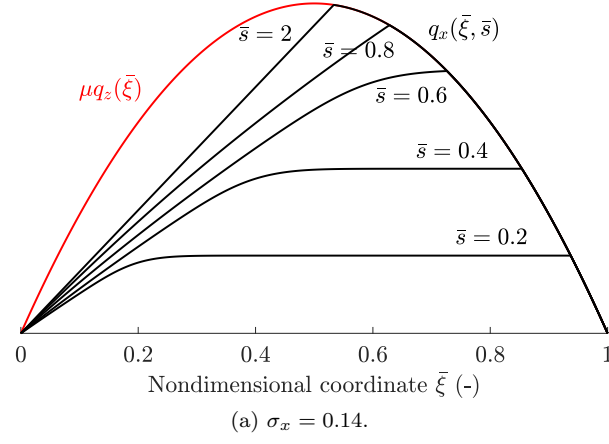(b) $\sigma_y = 0.14$, $\varphi = -0.07$.

Figure 5: Transient evolution of the lateral shear stresses for combined lateral slip and spin inputs with limited friction, for different values of the nondimensional travelled distance $\bar{s} = s/(2a)$. The solid and dashed lines refer to the analytical and numerical solutions, respectively. Tyre parameters: $F_z = 3000$ N, $k_x = k_y = k = 2.67 \cdot 10^6$ N m^{-2}, $C_x' = 6 \cdot 10^5$, $C_y' = 2.4 \cdot 10^5$ N m^{-1}, $a = 0.075$ m, $\mu = 1$.
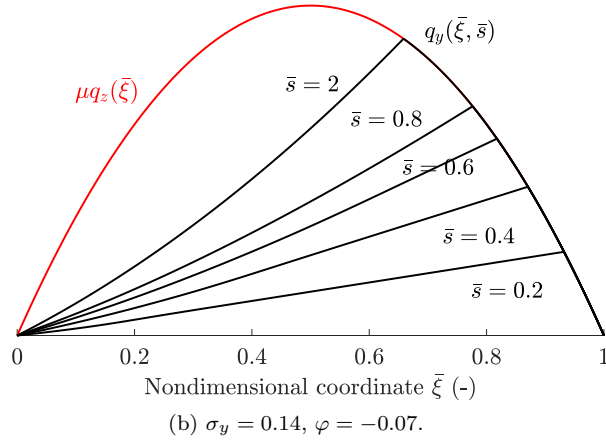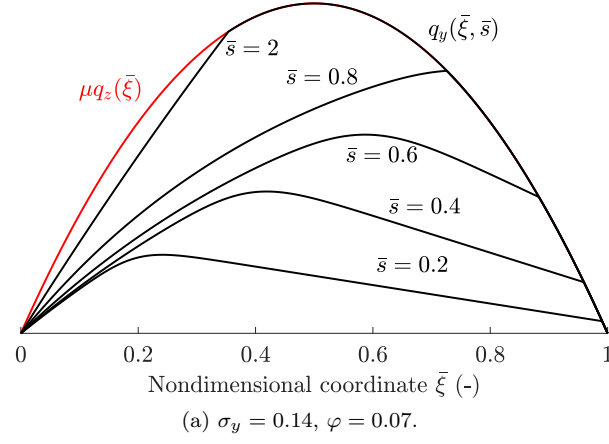
4 Transient LuGre-brush model

The LuGre-brush formulation provides the ideal theoretical framework to explore the more common situation of limited friction since, in contrast to the standard version of the brush models, the resulting equations governing the deflection of the bristles inside the contact patch do not differentiate between stick and slip conditions. Hence, the present section explores transient phenomena within the theoretical framework of the LuGre-brush models. First, Sect. 4.1 introduces the formulation with rigid carcass, for which some new analytical results are established. Then, Sect. 4.2 is dedicated to the more complex variant that accounts for the contribution of a flexible carcass. Finally, Sect. 4.3 is devoted to the derivation of lumped approximations to be used for vehicle control applications.

4.1 LuGre-brush model with rigid carcass

As for the standard version of the brush models, the analysis carried out in the present section is propaedeutic to the more complex situation of a flexible carcass. Moreover, general solutions that account for time-varying slip and spin inputs have not been reported in the literature. In particular, in the case of rigid tyre carcass, i.e., $\boldsymbol{\sigma}'(s) \equiv \boldsymbol{\sigma}(s)$, the governing PDEs of the model simplify clearly to

$$\frac{\partial \boldsymbol{z}(\xi,s)}{\partial s} + \frac{\partial \boldsymbol{z}(\xi,s)}{\partial \xi} = \boldsymbol{\sigma}(s) + \mathbf{A}_\varphi(s)\begin{bmatrix} a-\xi \\ 0 \end{bmatrix} - \frac{\hat{v}_\mu(s)}{V_{\mathrm{r}}(s)g(\hat{v}_\mu(s))}\mathbf{C}_0\boldsymbol{z}(\xi,s), \qquad (\xi,s) \in \mathring{\mathscr{P}} \times \mathbb{R}_{>0}, \quad (44)$$

with BC and IC reading as in Eqs. (17a) and (17b). Similarly as for the solution derived in Sect. 3.1, imposing the BC and IC yields two different expressions for the internal frictional state:

$$\boldsymbol{z}^-(\xi,s) = \int_0^\xi \boldsymbol{\Phi}_\mu(\xi,\xi',s)\left[\boldsymbol{\sigma}(\xi'-\xi+s) + \mathbf{A}_\varphi(\xi'-\xi+s)\begin{bmatrix} a-\xi' \\ 0 \end{bmatrix}\right]\mathrm{d}\xi', \quad (\xi,s) \in \mathscr{P}^- \times \mathbb{R}_{\geq 0}, \quad (45a)$$

$$\boldsymbol{z}^+(\xi,s) = \int_0^s \boldsymbol{\Phi}_\mu(s,s')\left[\boldsymbol{\sigma}(s') + \mathbf{A}_\varphi(s')\begin{bmatrix} a-s'+s-\xi \\ 0 \end{bmatrix}\right]\mathrm{d}s' + \boldsymbol{\Phi}_\mu(s,0)\boldsymbol{z}_0(\xi-s), \quad (\xi,s) \in \mathscr{P}^+ \times \mathbb{R}_{\geq 0}, \quad (45b)$$

in which the *Stribeck* transition matrix may be easily computed using matrix exponentiation as follows:

$$\boldsymbol{\Phi}_\mu(\xi,\tilde{\xi},s) = \mathrm{e}^{-\mathbf{C}_0 \int_{\tilde{\xi}}^\xi \frac{\hat{v}_\mu(\xi'-\xi+s)}{V_{\mathrm{r}}(\xi'-\xi+s)g(\hat{v}_\mu(\xi'-\xi+s))}\mathrm{d}\xi'}$$

$$= \begin{bmatrix} \exp\left(-\int_{\tilde{\xi}}^\xi \varphi_x(\xi'-\xi+s)\,\mathrm{d}\xi'\right) & 0 \\ 0 & \exp\left(-\int_{\tilde{\xi}}^\xi \varphi_y(\xi'-\xi+s)\,\mathrm{d}\xi'\right) \end{bmatrix}, \quad (46a)$$

$$\boldsymbol{\Phi}_\mu(s,\tilde{s}) = \mathrm{e}^{-\mathbf{C}_0 \int_{\tilde{s}}^s \frac{\hat{v}_\mu(s')}{V_{\mathrm{r}}(s')g(\hat{v}_\mu(s'))}\mathrm{d}s'} = \begin{bmatrix} \exp\left(-\int_{\tilde{s}}^s \varphi_x(s')\,\mathrm{d}s'\right) & 0 \\ 0 & \exp\left(-\int_{\tilde{s}}^s \varphi_y(s')\,\mathrm{d}s'\right) \end{bmatrix}, \quad (46b)$$

and the *dissipative curvatures* $\varphi_x(s)$, $\varphi_y(s)$ have been conveniently defined as

$$\varphi_x(s) \triangleq \frac{c_{0x}\hat{v}_\mu(s)}{V_{\mathrm{r}}(s)g(\hat{v}_\mu(s))}, \qquad \text{and} \qquad \varphi_y(s) \triangleq \frac{c_{0y}\hat{v}_\mu(s)}{V_{\mathrm{r}}(s)g(\hat{v}_\mu(s))}. \quad (47)$$

The complete solution over the contact patch may be then constructed in the same spirit of Eq. (23) by setting

$$\boldsymbol{z}(\xi,s) = \begin{cases} \boldsymbol{z}^-(\xi,s), & (\xi,s) \in \mathscr{P}^- \times \mathbb{R}_{\geq 0}, \\ \boldsymbol{z}^+(\xi,s), & (\xi,s) \in \mathscr{P}^+ \times \mathbb{R}_{\geq 0}. \end{cases} \quad (48)$$

For the LuGre-brush model with rigid tyre carcass, the conclusions about the regularity of the weak solution derived in Eqs. (45), (46), (47) and (48) are similar to those already drawn in Sect. 3.1. Concerning the physical nature of the transient process of generation of tyre forces and moment, however, the response predicted by the LuGre-brush formulation is substantially different from that described by the standard version of the brush models. This should be ascribed to the presence of the dissipative term in Eqs. (44), which acts as an additional damping effect. As a result, the contribution of the initial conditions to the total deflection of the bristles decreases exponentially in time (or over travelled distance),

determining a different rate of convergence to the steady-state behaviour. This may be also understood by looking at the analytical expressions for the solution $z^+(\xi, s)$ derived for the case of constant slip inputs, and reported in [77].

In any case, input-to-state stability estimates in the form of Eqs. (24) may be derived directly from the closed-form expressions in (44), since the dissipative curvatures $\varphi_x(s)$, $\varphi_y(s)$ are, by definition, always nonnegative.

4.2   LuGre-brush model with flexible carcass

When considering a compliant carcass, the structure of the model changes depending on the specific assumption made about the matrices $\mathbf{C}_1$ and $\mathbf{C}_2$ appearing in Eq. (18). As a result, the two different conditions $\mathbf{C}_1 + \mathbf{C}_2 = \mathbf{0}$ and $\mathbf{C}_1 + \mathbf{C}_2 \neq \mathbf{0}$ require dedicated investigations, and must be addressed separately.

In what follows, results about existence and uniqueness of the solution are derived for both cases. On the other hand, a proper stability analysis similar to that presented in Sect. 3.2.2 is not attempted for the LuGre-brush model, the fundamental reason being that the dissipative term – which depends upon the slip and spin inputs – does not admit any constant upper bound which is independent of the interval $[0, S]$, and moreover makes it inherently difficult to establish input-to-state estimate inequalities in standard form [84]. Instead, the notion of well-posedness is promptly exploited to validate the simplified lumped formulations developed in the subsequent Sect. 4.3.

4.2.1   Case I: $\mathbf{C}_1 + \mathbf{C}_2 = \mathbf{0}$

The first variant of the LuGre-brush model with flexible carcass assumes that all the entries of the matrices $\mathbf{C}_1$ and $\mathbf{C}_2$ are constantly equal to zero, and therefore also $\mathbf{C}_1 + \mathbf{C}_2 = \mathbf{0}$. In this case, differentiating Eq. (20a) with respect to the travelled distance s, and substituting Eqs. (18) and (14) into the resulting expression yields the following vector-valued ODE for the time-varying tangential forces:

$$
\begin{aligned}
\frac{\mathrm{d}\boldsymbol{F_t}(s)}{\mathrm{d}s} = \hat{\boldsymbol{F}}_{\boldsymbol{t}}^{\mathrm{I}}\big(\boldsymbol{z}(\cdot, s), s\big) &\triangleq \big(\mathbf{I} + \mathbf{C}_0 \mathbf{S}' F_z\big)^{-1} \mathbf{C}_0 \Bigg(F_z \boldsymbol{\sigma}(s) + \int_0^{2a} \mathbf{A}_\varphi(s) \begin{bmatrix} a - \xi \\ 0 \end{bmatrix} q_z(\xi)\,\mathrm{d}\xi \Bigg) \\
&\quad - \big(\mathbf{I} + \mathbf{C}_0 \mathbf{S}' F_z\big)^{-1} \frac{\hat{v}_\mu(s)}{V_\mathrm{r}(s) g\big(\hat{v}_\mu(s)\big)} \mathbf{C}_0 \mathbf{C}_0 \int_0^{2a} \boldsymbol{z}(\xi, s) q_z(\xi)\,\mathrm{d}\xi \\
&\quad - \big(\mathbf{I} + \mathbf{C}_0 \mathbf{S}' F_z\big)^{-1} \mathbf{C}_0 \boldsymbol{z}(2a, s) q_z(2a) \\
&\quad + \big(\mathbf{I} + \mathbf{C}_0 \mathbf{S}' F_z\big)^{-1} \mathbf{C}_0 \int_0^{2a} \boldsymbol{z}(\xi, s) \frac{\mathrm{d}q_z(\xi)}{\mathrm{d}\xi}\,\mathrm{d}\xi, \quad s \in (0, S).
\end{aligned}
\tag{49}
$$

Inserting Eq. (49) into the original PDEs (14) then gives

$$
\begin{aligned}
\frac{\partial \boldsymbol{z}(\xi, s)}{\partial s} + \frac{\partial \boldsymbol{z}(\xi, s)}{\partial \xi} &= \boldsymbol{\sigma}(s) + \mathbf{A}_\varphi(s) \begin{bmatrix} a - \xi \\ 0 \end{bmatrix} - \frac{\hat{v}_\mu(s)}{V_\mathrm{r}(s) g\big(\hat{v}_\mu(s)\big)} \mathbf{C}_0 \boldsymbol{z}(\xi, s) \\
&\quad - \mathbf{S}' \hat{\boldsymbol{F}}_{\boldsymbol{t}}^{\mathrm{I}}\big(\boldsymbol{z}(\cdot, s), s\big), \quad (\xi, s) \in \mathring{\mathscr{P}} \times (0, S),
\end{aligned}
\tag{50}
$$

with BC and IC given by Eqs. (17a) and (17b). It should be observed that, assuming $\mathbf{C}_1 + \mathbf{C}_2 = \mathbf{0}$, the transient dynamics of the tyre with compliant carcass is entirely described by a system of two PDEs with nonlocal terms. Clearly, the expression for the function $\hat{\boldsymbol{F}}_{\boldsymbol{t}}^{\mathrm{I}}(\cdot, \cdot)$ appearing in Eqs. (49) and (50) simplifies if the vertical pressure distribution is supposed to be constant over the contact patch, or alternatively $q_z \in C^1([0, 2a]; \mathbb{R})$ with $q_z(0) = q_z(2a) = 0$. Both assumptions are standard in the literature.

The following Theorem 4.1 establishes the main result for the well-posedness of the problem described by Eq. (50).

Theorem 4.1 (Existence and uniqueness of the solution for the LuGre-brush model with flexible carcass (Case I)). *Under the assumption $(\boldsymbol{\sigma}, \varphi) \in C^0([0, S]; \mathbb{R}^3)$, $V_\mathrm{r} \in C^0([0, S]; \mathbb{R}_{>0})$, $\hat{v}_\mu \in C^0([0, S]; \mathbb{R})$, and $\boldsymbol{z}_0 \in C^0(\mathscr{P}; \mathbb{R}^2)$, Eq. (50) equipped with BC (17a) and IC (17b) admits a unique solution $\boldsymbol{z} \in$*

$C^0(\mathscr{P} \times [0,S]; \mathbb{R}^2)$ *in the form of Eq.* (48)*, with* $\boldsymbol{z}^-(\xi,s)$ *and* $\boldsymbol{z}^+(\xi,s)$ *satisfying*

$$\boldsymbol{z}^-(\xi,s) = \int_0^\xi \boldsymbol{\Phi}_\mu(\xi,\xi',s)\left[\boldsymbol{\sigma}(\xi'-\xi+s) + \mathbf{A}_\varphi(\xi'-\xi+s)\begin{bmatrix} a-\xi' \\ 0 \end{bmatrix}\right]\mathrm{d}\xi'$$

$$-\int_0^\xi \boldsymbol{\Phi}_\mu(\xi,\xi',s)\mathbf{S}'\hat{\boldsymbol{F}}_{\boldsymbol{t}}^{\mathrm{I}}\Big(\boldsymbol{F}_{\boldsymbol{t}}(\xi'-\xi+s), \boldsymbol{z}(\cdot,\xi'-\xi+s), \xi'-\xi+s\Big)\mathrm{d}\xi', \quad (\xi,s) \in \mathscr{P}^- \times [0,S],$$

$$\tag{51a}$$

$$\boldsymbol{z}^+(\xi,s) = \int_0^s \boldsymbol{\Phi}_\mu(s,s')\left[\boldsymbol{\sigma}(s') + \mathbf{A}_\varphi(s')\begin{bmatrix} a-s'+s-\xi \\ 0 \end{bmatrix}\right]\mathrm{d}s'$$

$$-\int_0^s \boldsymbol{\Phi}_\mu(s,s')\mathbf{S}'\hat{\boldsymbol{F}}_{\boldsymbol{t}}^{\mathrm{I}}\Big(\boldsymbol{F}_{\boldsymbol{t}}(s'), \boldsymbol{z}(\cdot,s'), s'\Big)\mathrm{d}s' + \boldsymbol{\Phi}_\mu(s,0)\boldsymbol{z}_0(\xi-s), \quad (\xi,s) \in \mathscr{P}^+ \times [0,S],$$

$$\tag{51b}$$

in which the Stribeck transition matrix reads as in Eq. (46)*.*

Proof. The proof is similar to those of Theorems 3.1 and 4.2, and hence omitted for brevity. $\qquad\square$

4.2.2 Case II: $\mathbf{C}_1 + \mathbf{C}_2 \neq \mathbf{0}$

If at least one of the matrices $\mathbf{C}_1$ and $\mathbf{C}_1$ is positive definite, the derivative of the tyre forces may be expressed directly as a function of the internal frictional state $\boldsymbol{z}(\xi,s)$ by combining Eqs. (18) and (20a) with (14), i.e., without the need for deriving Eq. (20a). Similar manipulations as those performed in Sect. 4.2.1 then provide the following PDE-ODE loop:

$$\frac{\mathrm{d}\boldsymbol{F}_{\boldsymbol{t}}(s)}{\mathrm{d}s} = \hat{\boldsymbol{F}}_{\boldsymbol{t}}^{\mathrm{II}}\big(\boldsymbol{F}_{\boldsymbol{t}}(s), \boldsymbol{z}(\cdot,s), s\big), \quad s \in (0,S), \tag{52a}$$

$$\frac{\partial \boldsymbol{z}(\xi,s)}{\partial s} + \frac{\partial \boldsymbol{z}(\xi,s)}{\partial \xi} = \boldsymbol{\sigma}(s) + \mathbf{A}_\varphi(s)\begin{bmatrix} a-\xi \\ 0 \end{bmatrix} - \frac{\hat{v}_\mu(s)}{V_\mathrm{r}(s)g(\hat{v}_\mu(s))}\mathbf{C}_0\boldsymbol{z}(\xi,s)$$

$$- \mathbf{S}'\hat{\boldsymbol{F}}_{\boldsymbol{t}}^{\mathrm{II}}\big(\boldsymbol{F}_{\boldsymbol{t}}(s), \boldsymbol{z}(\cdot,s), s\big), \quad (\xi,s) \in \mathring{\mathscr{P}} \times (0,S), \tag{52b}$$

where

$$\hat{\boldsymbol{F}}_{\boldsymbol{t}}^{\mathrm{II}}\big(\boldsymbol{F}_{\boldsymbol{t}}(s), \boldsymbol{z}(\cdot,s), s\big) \triangleq -\frac{\mathbf{C}'}{V_\mathrm{r}(s)F_z}(\mathbf{C}_1+\mathbf{C}_2)^{-1}\boldsymbol{F}_{\boldsymbol{t}}(s) + \mathbf{C}'\boldsymbol{\sigma}(s) + \frac{\mathbf{C}'}{F_z}\int_0^{2a} \mathbf{A}_\varphi(s)\begin{bmatrix} a-\xi \\ 0 \end{bmatrix}q_z(\xi)\,\mathrm{d}\xi$$

$$+ \frac{\mathbf{C}'}{V_\mathrm{r}(s)F_z}(\mathbf{C}_1+\mathbf{C}_2)^{-1}\left(\mathbf{I} - \frac{\hat{v}_\mu(s)}{g(\hat{v}_\mu(s))}\mathbf{C}_1\right)\mathbf{C}_0\int_0^{2a} \boldsymbol{z}(\xi,s)q_z(\xi)\,\mathrm{d}\xi \tag{53}$$

$$- \frac{\mathbf{C}'}{F_z}(\mathbf{C}_1+\mathbf{C}_2)^{-1}\mathbf{C}_1\left(\boldsymbol{z}(2a,s)q_z(2a) - \int_0^{2a} \boldsymbol{z}(\xi,s)\frac{\mathrm{d}q_z(\xi)}{\mathrm{d}\xi}\,\mathrm{d}\xi\right).$$

As opposed to the model derived previously in Sect. 4.2.1 for the case $\mathbf{C}_1 + \mathbf{C}_2 = \mathbf{0}$, Eqs. (52) describe the transient dynamics of the tyre by means of a system of interconnected PDE-ODEs. Accordingly, whilst the BC and IC for Eq. (52b) read again as in (17a) and (17b), Eq. (52a) should be supplemented by an appropriate IC. In particular, the compatibility condition between the initial value $\boldsymbol{F}_{\boldsymbol{t}0}$ for the tangential tyre forces and the initial distribution $\boldsymbol{z}_0(\xi)$ for the internal frictional variable yields

$$\text{IC:} \qquad \boldsymbol{F}_{\boldsymbol{t}}(0) = \boldsymbol{F}_{\boldsymbol{t}0} = \int_{\mathscr{P}}\big(\mathbf{C}_0\boldsymbol{z}_0(\xi) + \mathbf{C}_2\hat{v}_\mu(0)\big)q_z(\xi)\,\mathrm{d}\xi. \tag{54}$$

The corresponding existence and uniqueness result for the system described by Eqs. (52) and (53), and equipped with BC (17a) and ICs (17b), (54) is asserted in the following Theorem (4.2).

Theorem 4.2 (Existence and uniqueness of the solution for the LuGre-brush model with flexible carcass (Case II))**.** *Under the assumption* $(\boldsymbol{\sigma},\varphi) \in C^0([0,S];\mathbb{R}^3)$, $V_\mathrm{r} \in C^0([0,S];\mathbb{R}_{>0})$, $\hat{v}_\mu \in C^0([0,S];\mathbb{R})$, *and* $\boldsymbol{z}_0 \in C^0(\mathscr{P};\mathbb{R}^2)$, *Eqs. equipped with BC* (17a) *and ICs* (17b)*,* (54) *admit unique solutions* $\boldsymbol{F}_{\boldsymbol{t}} \in$

$C^1([0, S]; \mathbb{R}^2)$ *and* $\boldsymbol{z} \in C^0(\mathscr{P} \times [0, S]; \mathbb{R}^2)$ *in the form of Eq.* (48), *with* $\boldsymbol{z}^-(\xi, s)$ *and* $\boldsymbol{z}^+(\xi, s)$ *satisfying*

$$\boldsymbol{z}^-(\xi, s) = \int_0^\xi \boldsymbol{\Phi}_\mu(\xi, \xi', s) \left[\boldsymbol{\sigma}(\xi' - \xi + s) + \mathbf{A}_\varphi(\xi' - \xi + s) \begin{bmatrix} a - \xi' \\ 0 \end{bmatrix} \right] \mathrm{d}\xi'$$

$$- \int_0^\xi \boldsymbol{\Phi}_\mu(\xi, \xi', s) \mathbf{S}' \hat{\boldsymbol{F}}_{\boldsymbol{t}}^{\mathrm{II}} \Big(\boldsymbol{F}_{\boldsymbol{t}}(\xi' - \xi + s), \boldsymbol{z}(\cdot, \xi' - \xi + s), \xi' - \xi + s \Big) \mathrm{d}\xi', \quad (\xi, s) \in \mathscr{P}^- \times [0, S],$$

(55a)

$$\boldsymbol{z}^+(\xi, s) = \int_0^s \boldsymbol{\Phi}_\mu(s, s') \left[\boldsymbol{\sigma}(s') + \mathbf{A}_\varphi(s') \begin{bmatrix} a - s' + s - \xi \\ 0 \end{bmatrix} \right] \mathrm{d}s'$$

$$- \int_0^s \boldsymbol{\Phi}_\mu(s, s') \mathbf{S}' \hat{\boldsymbol{F}}_{\boldsymbol{t}}^{\mathrm{II}} \Big(\boldsymbol{F}_{\boldsymbol{t}}(s'), \boldsymbol{z}(\cdot, s'), s' \Big) \mathrm{d}s' + \boldsymbol{\Phi}_\mu(s, 0) \boldsymbol{z}_0(\xi - s), \quad (\xi, s) \in \mathscr{P}^+ \times [0, S],$$

(55b)

in which the Stribeck transition matrix reads as in Eq. (46).

Proof. See Appendix A.2. □

The transient response predicted by the two different variants of the LuGre-brush models are compared in Fig. 6, where the distribution of the stresses $\mu_x(\xi, s) q_z(\xi)$ and $\mu_y(\xi, s) q_z(\xi)$ are plotted for a tyre subjected to pure longitudinal and lateral slip inputs $\sigma_x = \sigma_y = 0.14$, departing from an initial undeformed configuration $\boldsymbol{z}_0(\xi) = \boldsymbol{0}$, and for different values of the nondimensional travelled distance $\bar{s} = s/(2a)$. In Fig. 6, the vertical pressure distribution is modelled with a parabolic trend. Generally speaking, it may be observed that the model derived for the case $\mathbf{C}_1 + \mathbf{C}_2 \neq \boldsymbol{0}$ (dashed lines) predicts a slower response for relatively small values of the nondimensional travelled distance. For a fixed value of $\bar{s}$, the trend of the distributions $\mu_x(\xi, s) q_z(\xi)$ and $\mu_y(\xi, s) q_z(\xi)$ are however similar between the two models.

Once again, it may also be noticed that the response of the tyre in the lateral direction is slower, due to the fact that the carcass usually exhibits an anisotropic behaviour, and is more compliant laterally. Moreover, compared to the standard version of the brush models detailed in Sect. 3, it may be observed that, according to the LuGre-brush formulation, steady-state conditions are reached relatively faster, approximately after travelling a distance equal to the contact length. The discrepancy between the two predicted behaviours resides again in the presence of the dissipative term appearing in Eq. (14). The effect of small spin slips may also be analysed as done in Sect. 3, but is not discussed extensively in the present section for the sake of brevity.

4.3 Lumped LuGre-brush model with flexible carcass

The intuition preliminarily gained from the models derived and partially analysed in Sect. 4.2 may be used to develop lumped approximations to be used in vehicle dynamics simulation and control applications. This is a common approach in the dedicated literature [35–41], yielding a description of the transient dynamics of the tyre in terms of simplified systems of ODEs. Moreover, since the distributed formulations introduced in Sect. 4.2 have been proved to be well-posed, they may be used to validate the approximated descriptions derived in the following.

Again, two variants are obtained depending on which between the conditions $\mathbf{C}_1 + \mathbf{C}_2 = \boldsymbol{0}$ or $\mathbf{C}_1 + \mathbf{C}_2 \neq \boldsymbol{0}$ is verified. Interestingly, a similar structure to that of the models presented in Sects. 4.2.1 and 4.2.2, respectively, appears to be inherited also by their lumped counterparts.

4.3.1 Case I: $\mathbf{C}_1 + \mathbf{C}_2 = \boldsymbol{0}$

If the condition $\mathbf{C}_1 + \mathbf{C}_2 = \boldsymbol{0}$ is fulfilled, a lumped approximation may be derived by first defining the averaged state $\hat{\boldsymbol{z}}(s) = [\hat{z}_x(s) \ \hat{z}_y(s)]^\mathrm{T}$ as

$$\hat{\boldsymbol{z}}(s) \triangleq \frac{1}{F_z} \int_0^{2a} \boldsymbol{z}(\xi, s) q_z(s) \, \mathrm{d}\xi,$$

(56)

which, owing to the assumption $\mathbf{C}_1 = \mathbf{C}_2 = \boldsymbol{0}$, also implies

$$\boldsymbol{F}_{\boldsymbol{t}}(s) = F_z \mathbf{C}_0 \hat{\boldsymbol{z}}(s).$$

(57)

(a) $\sigma_x = 0.14$.

(b) $\sigma_y = 0.14$.
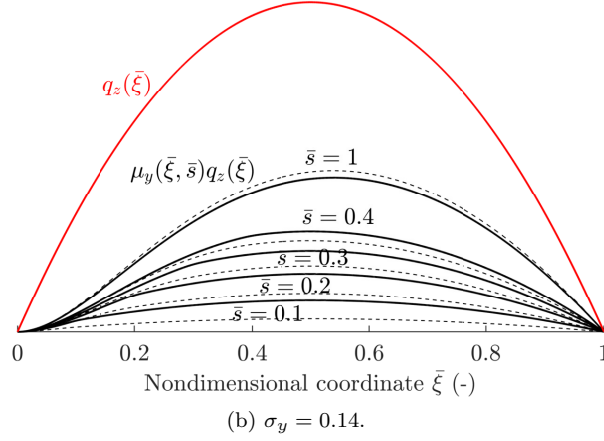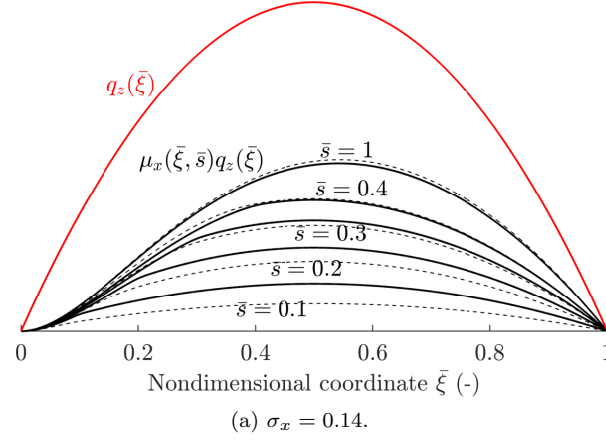
Figure 6: Transient evolution of the tangential shear stresses according to the LuGre-brush model with flexible carcass for a tyre subjected to pure longitudinal and lateral slip inputs, for different values of the nondimensional travelled distance $\bar{s} = s/(2a)$. The solid lines represent the solution obtained for the case $\mathbf{C}_1 + \mathbf{C}_0 = \mathbf{0}$, whereas the dotted lines to that obtained for the case $\mathbf{C}_1 + \mathbf{C}_2 \neq \mathbf{0}$. Tyre parameters: $F_z = 3000$ N, $V_\mathrm{r} = 20$ m s^{-1}, $v_\delta = 3.49$ m s^{-1}, $\delta = 0.6$, $c_{0x} = c_{0y} = 133$ m^{-1}, $c_{1x} = c_{1y} = 0.15$ s m^{-1} (for the model in Case II), $c_{2x} = c_{2y} = 0$ s m^{-1}, $C'_x = 6 \cdot 10^5$, $C'_y = 2.4 \cdot 10^5$ N m^{-1}, $a = 0.075$ m, $\mu_\mathrm{s} = 1$, $\mu_\mathrm{d} = 0.7$.

Differentiating Eq. (56) with respect to the travelled distance gives

$$
\begin{aligned}
\frac{\mathrm{d}\hat{\boldsymbol{z}}(s)}{\mathrm{d}s} &= \frac{1}{F_z} \int_0^{2a} \frac{\partial \boldsymbol{z}(\xi,s)}{\partial s} q_z(\xi)\,\mathrm{d}\xi = -\big(\mathbf{I} + F_z \mathbf{S}' \mathbf{C}_0\big)^{-1} \left(\frac{\hat{v}_\mu(s)}{V_\mathrm{r}(s) g\big(\hat{v}_\mu(s)\big)} \mathbf{C}_0 + \mathbf{K}(s) \right) \hat{\boldsymbol{z}}(s) \\
&\quad + \big(\mathbf{I} + F_z \mathbf{S}' \mathbf{C}_0\big)^{-1} \left(\boldsymbol{\sigma}(s) + \frac{1}{F_z} \int_0^{2a} \mathbf{A}_\varphi(s) \begin{bmatrix} a - \xi \\ 0 \end{bmatrix} q_z(\xi)\,\mathrm{d}\xi \right), \quad s \in \mathbb{R}_{>0},
\end{aligned}
\tag{58}
$$

where the matrix $\mathbf{K} \in \mathbb{R}^{2\times 2}$ is diagonal, i.e.,

$$
\mathbf{K}(s) = \begin{bmatrix} \kappa_x(s) & 0 \\ 0 & \kappa_y(s) \end{bmatrix},
\tag{59}
$$

with

$$
\kappa_x(s) \triangleq \frac{1}{\int_0^{2a} z_x(\xi,s) q_z(\xi)\,\mathrm{d}\xi} \left(z_x(2a,s) q_z(2a) - \int_0^{2a} z_x(\xi,s) \frac{\mathrm{d}q_z(\xi)}{\mathrm{d}\xi}\,\mathrm{d}\xi \right),
\tag{60a}
$$

$$
\kappa_y(s) \triangleq \frac{1}{\int_0^{2a} z_y(\xi,s) q_z(\xi)\,\mathrm{d}\xi} \left(z_y(2a,s) q_z(2a) - \int_0^{2a} z_y(\xi,s) \frac{\mathrm{d}q_z(\xi)}{\mathrm{d}\xi}\,\mathrm{d}\xi \right).
\tag{60b}
$$

In Eq. (60), the coefficients $\kappa_x(s)$ and $\kappa_y(s)$ are usually approximated by considering the steady-state expressions for the internal frictional state $\boldsymbol{z}(\xi,s)$, which guarantees that the lumped model yields the same values for the tyre characteristics, at least in stationary conditions. Extensive discussion about different methods to correctly choose the parameters $\kappa_x(s)$ and $\kappa_y(s)$ so as to preserve the dissipative nature of the original distributed formulation are reported, for example, in [35–41].

A similar equation may be derived concerning the self-aligning moment, by introducing

$$
\hat{z}_{yx}(s) \triangleq \frac{1}{aF_z} \int_0^{2a} \xi z_y(\xi,s) q_z(\xi)\,\mathrm{d}\xi,
\tag{61}
$$

so that

$$
M_z(s) = aF_z c_{0y}\big(\hat{z}_y(s) - \hat{z}_{yx}(s)\big).
\tag{62}
$$

Deriving Eq. (61) with respect to the travelled distance yields, in turn,

$$
\begin{aligned}
\frac{\mathrm{d}\hat{z}_{yx}(s)}{\mathrm{d}s} &= \frac{1}{aF_z} \int_0^{2a} \xi \frac{\partial z_y(\xi,s)}{\partial s} q_z(\xi)\,\mathrm{d}\xi = -\left(\frac{c_{0y}\hat{v}_\mu(s)}{V_\mathrm{r}(s) g\big(\hat{v}_\mu(s)\big)} + \kappa_{yx}(s) \right) \hat{z}_{yx}(s) \\
&\quad + \frac{1}{aF_z} \left(\sigma_y(s) - S_y' \frac{\mathrm{d}F_y(s)}{\mathrm{d}s} \right) \int_0^{2a} \xi q_z(\xi)\,\mathrm{d}\xi + \frac{\varphi(s)}{aF_z} \int_0^{2a} (a-\xi)\xi q_z(\xi)\,\mathrm{d}\xi, \quad s \in \mathbb{R}_{>0},
\end{aligned}
\tag{63}
$$

where the coefficient $\kappa_{yx}(s)$, reading

$$
\kappa_{yx}(s) \triangleq \frac{1}{\int_0^{2a} \xi z_y(\xi,s) q_z(s)\,\mathrm{d}\xi} \left(2a z_y(2a,s) q_z(2a) - \int_0^{2a} z_y(\xi,s)\left(q_z(\xi) + \xi \frac{\mathrm{d}q_z(\xi)}{\mathrm{d}\xi} \right)\mathrm{d}\xi \right),
\tag{64}
$$

may be chosen following similar considerations as for the parameters $\kappa_x(s)$ and $\kappa_y(s)$.

The ICs for the linear ODEs (58) and (63) may be inferred immediately from those imposed on the frictional variable. It is also interesting to notice that, according to Eq. (58), the transient dynamics of the tyre is completely described by the lumped state, whereas the tangential tyre forces do not enter the system of simplified ODEs. In this context, the structure of the approximated formulation resembles that of the original distributed model discussed in Sect. 4.2.1.

Figure 7 compares the transient respose of the tyre according to the original distributed model and the lumped approximation for the case $\mathbf{C}_1 + \mathbf{C}_2 = \mathbf{0}$, considering a parabolic pressure distribution, and for different values of slip and spin inputs. Concerning both the tangential forces and the self-aligning moment, it may be inferred that the simplified formulation captures quite well the exact trend. Different combinations of slip inputs, possibly time-varying, may also be analysed using numerical methods.
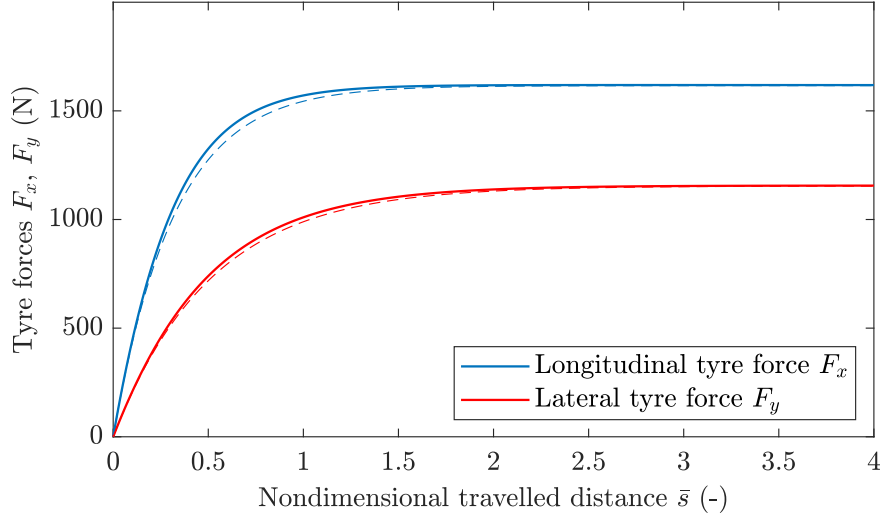
(a) $\sigma_x = 0.14$, $\sigma_y = 0.07$.
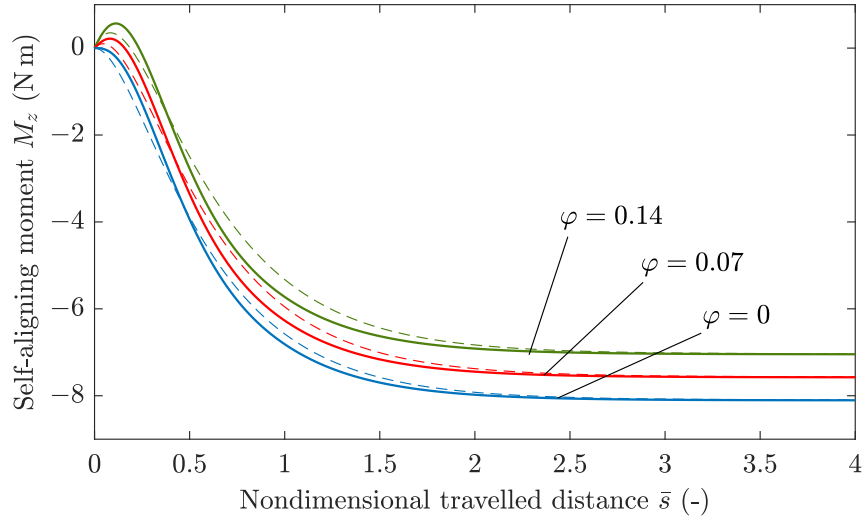
(b) $\sigma_y = 0.14$.

Figure 7: Transient evolution of the tangential tyre forces and moments for combined lateral slip and spin inputs. The solid and dashed lines refer to the original distributed model and to the lumped approximation, respectively. Tyre parameters: $F_z = 3000$ N, $V_r = 20$ m s^{-1}, $v_\delta = 3.49$ m s^{-1}, $\delta = 0.6$, $c_{0x} = c_{0y} = 133$ m^{-1}, $c_{1x} = c_{1y} = 0$ s m^{-1}, $c_{2x} = c_{2y} = 0$ s m^{-1}, $C'_x = 6 \cdot 10^5$, $C'_y = 2.4 \cdot 10^5$ N m^{-1}, $a = 0.075$ m, $\mu_s = 1$, $\mu_d = 0.7$.

22

4.3.2 Case II: $\mathbf{C}_1 + \mathbf{C}_2 \neq \mathbf{0}$

When the condition $\mathbf{C}_1 + \mathbf{C}_2 \neq \mathbf{0}$ is verified, the lumped model may be derived by combining Eqs. (56) and (58) directly with (20a). In this case, the following ODE loop is obtained[5]:

$$
\begin{bmatrix} \dfrac{\mathrm{d}\boldsymbol{F_t}(s)}{\mathrm{d}s} \\[2mm] \dfrac{\mathrm{d}\hat{\boldsymbol{z}}(s)}{\mathrm{d}s} \end{bmatrix} = \begin{bmatrix} V_\mathrm{r}(s)F_z\mathbf{C}_2\mathbf{S}' & -V_\mathrm{r}(s)F_z\mathbf{C}_1 \\ \mathbf{S}' & \mathbf{I} \end{bmatrix}^{-1} \left(- \begin{bmatrix} \mathbf{I} & -F_z\mathbf{C_0} \\ \mathbf{0} & \dfrac{\hat{v}_\mu(s)}{V_\mathrm{r}(s)g(\hat{v}_\mu(s))}\mathbf{C_0} + \mathbf{K}(s) \end{bmatrix} \begin{bmatrix} \boldsymbol{F_t}(s) \\ \hat{\boldsymbol{z}}(s) \end{bmatrix} + \begin{bmatrix} \boldsymbol{f_{F_t}}(s) \\ \boldsymbol{f_{\hat{z}}}(s) \end{bmatrix} \right),
$$
$$
s \in \mathbb{R}_{>0},
$$
(65)

where

$$
\boldsymbol{f_{\hat{z}}}(s) \triangleq \boldsymbol{\sigma}(s) + \frac{1}{F_z} \int_0^{2a} \mathbf{A}_\varphi(s) \begin{bmatrix} a - \xi \\ 0 \end{bmatrix} q_z(\xi)\,\mathrm{d}\xi, \tag{66a}
$$

$$
\boldsymbol{f_{F_t}}(s) \triangleq V_\mathrm{r}(s)F_z\mathbf{C}_2\boldsymbol{f_{\hat{z}}}(s), \tag{66b}
$$

and the matrix $\mathbf{K}(s)$ reads as in Eq. (59), with $\kappa_x(s)$ and $\kappa_y(s)$ defined according to (60). Once again the ICs for the linear system (65) may be deduced from those prescribed for the original formulation. Similarly, in this case the transient dynamics of the tyre is approximated by an interconnection between a first set of ODEs for the tangential tyre forces, and a second one for the lumped state, in an obvious analogy to the model derived in Sect. 4.2.2.

The ODE for the variable $\hat{z}_{yx}(s)$ is formally identical to that derived in Sect. (4.3.1), with the dyamics of the lateral tyre force obeying instead the linear system (65). However, the self-aligning torque may be expressed in this case as

$$
M_z(s) = aF_z c_{0y}\big(\hat{z}_y(s) - \hat{z}_{yx}(s)\big) + V_\mathrm{r}(s)aF_z c_{1y}\left(\frac{\mathrm{d}\hat{z}_y(s)}{\mathrm{d}s} - \frac{\mathrm{d}\hat{z}_{yx}(s)}{\mathrm{d}s} \right)
$$
$$
+ V_\mathrm{r}(s)c_{2y}\left(\sigma_y(s) - S_y' \frac{\mathrm{d}F_y(s)}{\mathrm{d}s} \right) \int_0^{2a} (a - \xi)q_z(\xi)\,\mathrm{d}\xi + V_\mathrm{r}(s)c_{2y}\varphi(s) \int_0^{2a} (a - \xi)^2 q_z(\xi)\,\mathrm{d}\xi. \tag{67}
$$

Again, a comparison between the original distributed model and the lumped approximation for the case $\mathbf{C}_1 + \mathbf{C}_2 \neq \mathbf{0}$ is illustrated in Fig. 8 for different combinations of translational slip and spin inputs, and assuming a parabolic pressure distribution. Also in this case, the simplified formulation captures the exact dynamics with sufficient accuracy. However, it should be noticed that imposing a discontinuous spin input φ implies that the self-aligning moment is discontinuous over the travelled distance, according to Eq. (67).

5   Conclusions

The present paper investigated the transient dynamics of distributed tyre models, i.e., described in terms of partial differential equations (PDEs), with a compliant carcass. The analysis conducted in the present work concerned the standard version of the brush theory, which is complemented by a simple Coulomb-Amontons friction model, and the modified LuGre-brush formulation, which is more idoneous for control-oriented applications. A rigorous analysis of such models had never been attempted in the literature dealing with the subject, principally because of the rather involved structure of their governing equations. Indeed, both variants describe the transient behaviour of the tyre through linear transport equations with nonlocal and boundary terms, possibly interconnected with systems of ordinary differential equations (ODEs) for the tangential tyre forces. Results about the existence and uniqueness of the solution were advocated in this paper concerning both versions of the brush models; additionally, with respect to the classic formulation, a closed-form solution for the transient deflection of the bristles was recovered under the assumption of vanishing sliding. More specifically, it was shown that the complete solution consists of an integral equation, involving only known functions, where the deformation at the trailing edge obeys a set of delay differential equations (DDEs). Concerning the standard brush models, an input-to-state stability analysis was also conducted, in order to highlight the interesting relationship existing with the two-regime formulation already proposed by the authors in previous works [4, 33].

---

[5]It is worth to emphasise that the fulfilment of the condition $\mathbf{C}_1 + \mathbf{C}_2 \neq \mathbf{0}$ ensures that the first matrix on the right-hand side of Eq. (65) is never singular.
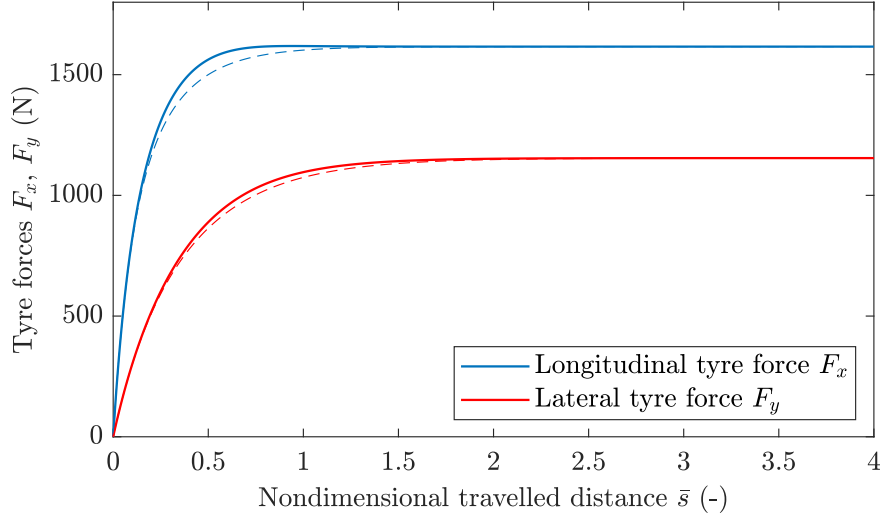
(a) $\sigma_x = 0.14$, $\sigma_y = 0.07$.
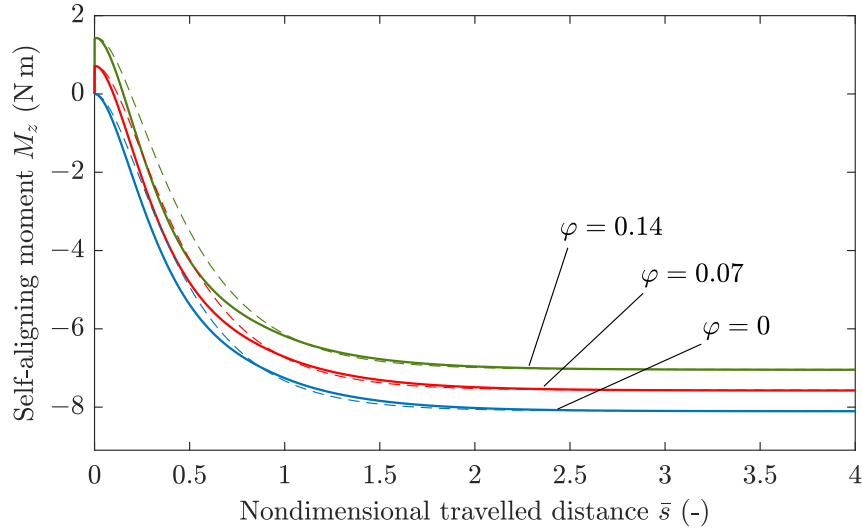
(b) $\sigma_y = 0.14$.

Figure 8: Transient evolution of the tangential tyre forces and moments for combined lateral slip and spin inputs. The solid and dashed lines refer to the original distributed model and to the lumped approximation, respectively. Tyre parameters: $F_z = 3000$ N, $V_r = 20$ m s^{-1}, $v_\delta = 3.49$ m s^{-1}, $\delta = 0.6$, $c_{0x} = c_{0y} = 133$ m^{-1}, $c_{1x} = c_{1y} = 0.015$ s m^{-1}, $c_{2x} = c_{2y} = 0$ s m^{-1}, $C'_x = 6 \cdot 10^5$, $C'_y = 2.4 \cdot 10^5$ N m^{-1}, $a = 0.075$ m, $\mu_s = 1$, $\mu_d = 0.7$.

While the case of limited friction was discussed only qualitatively within the theoretical framework provided by the classic version of the brush models, the modified LuGre-brush formulation offered an opportunity to explore such conditions in higher detail. In particular, it was shown that the mathematical structure of the governing equations for the LuGre-brush models with flexible carcass depends on the assumptions made on the matrices of curvatures $\mathbf{C}_1$ and $\mathbf{C}_2$. Accordingly, a first description may be derived solely in terms of PDEs if the condition $\mathbf{C}_1 + \mathbf{C}_2 = \mathbf{0}$ is satisfied, whereas the fulfilment of the criterion $\mathbf{C}_1 + \mathbf{C}_2 \neq \mathbf{0}$ yields a more involved interconnected system of PDE-ODEs. Both models may be effectively used to investigate the response of the tyre to time-varying slip input, to gain a fundamental intuition about the main phenomena responsible for the transient process of generation of forces and moment. Departing from these distributed representations, lumped approximations, consisting of simpler systems of linear ODEs, were also derived to facilitate the design and synthesis of controllers and estimators for vehicle dynamics application. The approximated models were validated against the original formulations, showing an encouragingly good agreement.

Despite the analysis conducted in the paper, the novel distributed formulations still require validation. In particular, the ability of the presented models to capture the transient behaviour of the tyre will need to be evaluated by performing specifically designed experiments. This is deferred to future research. Further efforts may be conveniently directed to exploring the potential of the new lumped formulation for the development of *ad-hoc* control algorithms. Moreover, the original formulations may be employed to conduct preliminary stability analysis of simplified vehicle models, e.g, single-track models, with distributed tyre representations.

Acknowledgements

Compliance with Ethical Standards

The authors declare that they have no conflict of interest.

Nomenclature

Forces and Moments	Unit	Description
$\boldsymbol{F_t}$	N	Tangential force vector
$\boldsymbol{F_{t0}}$	N	Initial conditions for the tangential force vector
F_x, F_y	N	Longitudinal and lateral tyre forces
F_{x0}, F_{y0}	N	Initial conditions for the longitudinal and lateral tyre forces
F_z	N	Vertical force
M_z	N m	Self-aligning moment
$\boldsymbol{q_t}$	$\mathrm{N\,m^{-2}}$	Tangential shear stress vector
q_t	$\mathrm{N\,m^{-2}}$	Total tangential shear stress
q_x, q_y	$\mathrm{N\,m^{-2}}$	Longitudinal and lateral shear stress
q_z	$\mathrm{N\,m^{-2}}$	Vertical pressure

Displacements	Unit	Description
$\boldsymbol{u_t}$	m	Vector of bristle deflections
u_x, u_y	m	Longitudinal and lateral deflection of the bristle
$\boldsymbol{u_t^-}$	m	Vector of steady-state bristle deflections
u_x^-, u_y^-	m	Steady-state longitudinal and lateral deflection of the bristle
$\boldsymbol{u_t^+}$	m	Vector of transient bristle deflections
u_x^+, u_y^+	m	Transient longitudinal and lateral deflection of the bristle
$\boldsymbol{u_{t0}}$	m	Initial conditions for the bristle deflection (IC)
u_{x0}, u_{y0}	m	Initial conditions for longitudinal and lateral displacement (IC)
$\boldsymbol{\delta_t}$	m	Tyre carcass tangential displacement vector

δ_x, δ_y	m	Tyre carcass longitudinal and lateral displacements

Frictional states	**Unit**	**Description**
$\boldsymbol{z}$	m	Internal frictional state vector
z_x, z_y	m	Longitudinal and lateral frictional states
$\boldsymbol{z}^-$	m	Steady-state frictional state vector
z_x^-, z_y^-	m	Steady-state longitudinal and lateral frictional states
$\boldsymbol{z}^+$	m	Transient frictional state vector
z_x^+, z_y^+	m	Transient longitudinal and lateral frictional states
$\hat{\boldsymbol{z}}$	m	Aggregate internal frictional state vector for tyre forces
$\hat{z}_x$, $\hat{z}_y$	m	Aggregate longitudinal and lateral frictional states for tyre forces
$\hat{z}_{yx}$	m	Aggregate frictional state for self-aligning moment

Coordinates	**Unit**	**Description**
s	m	Travelled distance
ξ	m	Longitudinal coordinate

Speeds	**Unit**	**Description**
$\boldsymbol{V}_{\mathrm{s}}$	$\mathrm{m\,s^{-1}}$	Sliding velocity
$V_{\mathrm{s}x}$, $V_{\mathrm{s}y}$	$\mathrm{m\,s^{-1}}$	Longitudinal and lateral sliding speeds
$\boldsymbol{V}_{\mathrm{s}}'$	$\mathrm{m\,s^{-1}}$	Transient sliding velocity
$V_{\mathrm{s}x}'$, $V_{\mathrm{s}y}'$	$\mathrm{m\,s^{-1}}$	Transient longitudinal and lateral sliding speeds
$\bar{\boldsymbol{v}}_{\mathrm{s}}$	-	Nondimensional micro-sliding velocity
$\bar{v}_{\mathrm{s}x}$, $\bar{v}_{\mathrm{s}y}$	-	Nondimensional longitudinal and lateral micro-sliding speeds
v_δ	$\mathrm{m\,s^{-1}}$	Stribeck velocity
$\hat{\boldsymbol{v}}_\mu$	$\mathrm{m\,s^{-1}}$	Average micro-sliding velocity
$\hat{v}_{\mu x}$, $\hat{v}_{\mu y}$	-	Average longitudinal and lateral micro-sliding speeds
$\hat{v}_\mu$	-	Total average micro-sliding velocity
V_{r}	$\mathrm{m\,s^{-1}}$	Tyre rolling speed

Slip Parameters	**Unit**	**Description**
$\boldsymbol{\sigma}$	-	Translational slip vector
σ_x, σ_y	-	Longitudinal and lateral slip
$\boldsymbol{\sigma}'$	-	Transient translational slip vector
σ_x, σ_y	-	Transient longitudinal and lateral slip
φ	$\mathrm{m^{-1}}$	Rotational slip or spin parameter

Rotational Matrices and Transition Matrices	**Unit**	**Description**
$\mathbf{A}_\varphi$	$\mathrm{m^{-1}}$	Spin tensor
φ_x, φ_y	$\mathrm{m^{-1}}$	Dissipative curvatures
$\boldsymbol{\Phi}_\mu$	-	Stribeck transition matrix
$\boldsymbol{\Phi}_{\boldsymbol{\sigma}'}$	-	Transient slip transition matrix

Geometric Parameters	**Unit**	**Description**
a	m	Contact patch semilength
λ_{σ_x}', λ_{σ_y}'	m	Longitudinal and lateral enhanced relaxation lengths

Curvature Matrices	**Unit**	**Description**
$\mathbf{C}_0$	$\mathrm{m^{-1}}$	Zeroth-order frictional matrix
c_{0x}, c_{0y}	$\mathrm{m^{-1}}$	Diagonal entries of the zeroth-order frictional matrix
$\mathbf{C}_1$	$\mathrm{s\,m^{-1}}$	First-order frictional matrix
c_{1x}, c_{1y}	$\mathrm{s\,m^{-1}}$	Diagonal entries of the first-order frictional matrix

$\mathbf{C}_2$	$\mathrm{s\,m^{-1}}$	First-order frictional matrix
c_{2x}, c_{2y}	$\mathrm{s\,m^{-1}}$	Diagonal entries of the first-order frictional matrix
$\mathbf{K}$	$\mathrm{m^{-1}}$	Curvature functions matrix for lumped model for tyre forces
k_x, k_y	$\mathrm{m^{-1}}$	Diagonal curvature functions matrix for tyre forces
k_{yx}	$\mathrm{m^{-1}}$	Curvature function for self-aligning moment

Stiffnesses and Compliances	Unit	Description
$\mathbf{K_t}$	$\mathrm{N\,m^{-2}}$	Matrix of tangential stiffnesses of the tread bristle
k_x, k_y	$\mathrm{N\,m^{-2}}$	Longitudinal and lateral stiffness of the tread bristle
$\mathbf{C}'$	$\mathrm{N\,m^{-1}}$	Matrix of tyre carcass stiffnesses
C_x', C_y'	$\mathrm{N\,m^{-1}}$	Longitudinal and lateral stiffness of the tyre carcass
$\mathbf{S}'$	$\mathrm{m\,N^{-1}}$	Matrix of tyre carcass compliances
S_x', S_y'	$\mathrm{m\,N^{-1}}$	Longitudinal and lateral compliance of the tyre carcass

Frictional Parameters	Unit	Description
μ	-	Friction coefficient
$\boldsymbol{\mu}$	-	Shear contribution coefficient vector
μ_x, μ_y	-	Longitudinal and lateral shear contribution coefficients
μ_d	-	Dynamic friction coefficient
μ_s	-	Static friction coefficient

Sets	Unit	Description
$\mathscr{P}$	m	Contact patch
$\mathscr{P}^-$	m	Steady-state zone
$\mathscr{P}^+$	m	Transient zone
$\mathscr{P}^{(\mathrm{a})}$	m	Adhesion zone
$\mathscr{P}^{(\mathrm{s})}$	m	Sliding zone
$\mathring{\mathscr{P}}$	m	Interior of $\mathscr{P}$
$\mathbb{R}_{\geq 0}$	-	Set of positive real numbers (including 0)
$\mathbb{R}_{> 0}$	-	Set of strictly positive real numbers (excluding 0)

References

[1] Pacejka HB. Tire and vehicle dynamics. 3rd ed. Amsterdam: Elsevier/BH; 2012.

[2] Guiggiani M. The Science of Vehicle Dynamics, 3rd ed. Cham(Switzerland): Springer International; 2023. Available from: https://doi.org/10.1007/978-3-031-06461-6.

[3] Genovese A, Garofano D, Sakhnevych A, Timpone F, Farroni F. (2021). Static and Dynamic Analysis of Non-Pneumatic Tires Based on Experimental and Numerical Methods. Applied Sciences, 11(23), 11232.

[4] Romano L, Bruzelius F, Jacobson B. Unsteady-state brush theory. Vehicle Syst. Dyn. 2020; pages 1-29. Available from: https://doi.org/10.1080/00423114.2020.1774625.

[5] Carputo F, D'Andrea D, Risitano G, Sakhnevych A, Santonocito D, Farroni F. (2021). A Neural-Network-Based Methodology for the Evaluation of the Center of Gravity of a Motorcycle Rider. Vehicles, 3(3), 377-389.

[6] Savaresi SM, Tanelli M. Active Braking Control Systems Design for Vehicles. Springer-Verlag, London (2010). Available from: https://doi.org/10.1007/978-1-84996-350-3.

[7] Koopman J, Jeltsema D, Verhaegen M. Port-Hamiltonian description and analysis of the LuGre friction model. Simulation Modelling Practice and Theory. 2011;19(3):959-968. Available from: https://doi.org/10.1016/j.simpat.2010.11.008.

[8] Yu H, Qi Z, Duan J, Taheri S, Ma Y. Multiple model adaptive backstepping control for antilock braking system based on LuGre dynamic tyre model. International Journal of Vehicle Design. 2015;69(1-4):168-184.

[9] Hou X, Zhang J, Liu W, Ji Y. LuGre Model-based Longitudinal Ride Comfort Control of Vehicle during the Post-braking Phase. 2020 Chinese Automation Congress (CAC). 2020:7307-7313. Available from: https://doi.org/110.1109/CAC51589.2020.9327063.

[10] Sharifzadeh M, Akbari A, Timpone F and Daryani R. Vehicle tyre/road interaction modeling

and identification of its parameters using real-time trust-region methods. IFAC-PapersOnLine. 2016;49(3):111-116. Available from: https://doi.org/10.1016/j.ifacol.2016.07.019.

[11] Sharifzadeh M, Timpone F, Farnam A, Senatore A, Akbari A. (2017). Tyre-Road Adherence Conditions Estimation for Intelligent Vehicle Safety Applications. In: Boschetti, G., Gasparetto, A. (eds) Advances in Italian Mechanism Science. Mechanisms and Machine Science, vol 47. Springer, Cham. Available from: https://doi.org/10.1007/978-3-319-48375-7_42.

[12] Sharifzadeh M, Senatore A, Farnam A, Akbari A, Timpone F. A real-time approach to robust identification of tyre–road friction characteristics on mixed-μ roads. Vehicle Syst. Dyn. 2019;57(9):1338-136. Available from: https://doi.org/10.1080/00423114.2018.1504974.

[13] Shao L, Jin C, Lex C, Eichberger A. Nonlinear adaptive observer for side slip angle and road friction estimation. 2016 IEEE 55th Conference on Decision and Control (CDC), 6258-6265 (2016).

[14] Shao L, Lex C, Hackl A, Eichberger A. Road friction estimation using recursive total least squares. 2016 IEEE Intelligent Vehicles Symposium (IV), 533-538 (2016).

[15] Shao L, Jin C, Lex C, Eichberger A. Robust road friction estimation during vehicle steering. Vehicle Syst. Dyn. 57(4): 493-519 (2019).

[16] Shao L, Jin C, Eicheberger A, Lex C. Grid search based tire-road friction estimation. IEEE Access 8, 81506-81525 (2020).

[17] Villano E, Lenzo B, Sakhnevych A. Cross-combined UKF for vehicle sideslip angle estimation with a modified Dugoff tire model: design and experimental results. Meccanica 56(11): 2653-2668 (2021).

[18] Guo N, Zhang X, Zou Y, Lenzo B. A supervisory control strategy of distributed drive electric vehicles for coordinating handling, lateral stability, and energy efficiency. IEEE Transactions on Transportation Electrification 7(4): 2488-2504 (2021).

[19] Di Biase F, Lenzo B, Timpone F. Vehicle sideslip angle estimation for a heavy-duty vehicle via Extended Kalman Filter using a Rational tyre model. IEEE Access 8: 142120-142130 (2020).

[20] Lenzo B, Zanchetta M, Sorniotti A, et al. Yaw Rate and Sideslip Angle Control Through Single Input Single Output Direct Yaw Moment Control. IEEE Transactions on Control Systems Technology (2020).

[21] Sakhnevych A, Arricale VM, Bruschetta M. Investigation on the model-based control performance in vehicle safety critical scenarios with varying tyre limits. Sensors 21(16) (2021).

[22] Jaiswal M, Mavros G, Rahnejat H, King PD. Influence of tyre transience on anti-lock braking. Proceedings of the Institution of Mechanical Engineers, Part K: Journal of Multi-body Dynamics. 2010;224(1):1-17. Available from: https://doi.org/10.1243/14644193JMBD225.

[23] Joa E, Yi K, Hyun Y. Estimation of the tire slip angle under various road conditions without tire–road information for vehicle stability control. Control Engineering Practice. 2019;86:129-143. Available from: https://doi.org/10.1016/j.conengprac.2019.03.005.

[24] Higuchi A. Transient response of tyres at large wheel slip and camber [doctoral thesis]. Delft; 1997.

[25] Higuchi A, Pacejka HB. The relaxation length concept at large wheel slip and camber. Vehicle Syst. Dyn. 1997;25(sup001):50-64. Available from: https://doi.org/10.1080/00423119708969644.

[26] Pauwelussen JP. The Local Contact Between Tyre and Road Under Steady State Combined Slip Conditions. Vehicle Syst. Dyn. 2004;41(1):1-26. Available from: http://doi.org/10.1076/vesd.41.1.1.23406.

[27] Svendenius J, Wittenmark B. Brush tire model with increased flexibility. European Control Conference, Cambridge, UK; 2015. Available from: https://dx.doi.org/10.23919/ECC.2003.7085237.

[28] Svendenius J. Tire modelling and friction estimation [dissertation]. Lund; 2007.

[29] Svendenius J, Gäfvert M, Bruzelius F, Hultén J. Experimental validation of the brush tire model. Tire Science and Technology. 2009;37(2):122-137.

[30] Rill G. Sophisticated but quite simple contact calculation for handling tire models. Multibody Syst. Dyn. 2019;45:131-153. Available from: https://doi.org/10.1007/s11044-018-9629-4.

[31] Rill G. Road vehicle Dynamics: Fundamentals and Modeling with MATLAB®. 2nd Ed. CRC Press; Boca Raton, 2020.

[32] Shaju A, Pandey AK. Modelling transient response using PAC 2002-based tyre model. Vehicle Syst. Dyn. 2020. Available from: https://doi.org/10.1080/00423114.2020.1802048.

[33] Romano L, Bruzelius F, Hjort M, Jacobson B. Development and analysis of the two-regime transient tyre model for combined slip. Vehicle Syst. Dyn. 2022.

[34] Romano L. Advanced Brush Tyre Modelling. SpringerBriefs in Applied Sciences. Springer, Cham (2022). Available from: https://doi.org/10.1007/978-3-030-98435-9.

[35] Deur J. Modeling and Analysis of Longitudinal Tire Dynamics Based on the Lugre Friction Model. IFAC Proceedings Volumes. 2001;34(1):91-96. Available from: https://doi.org/10.1016/

`S1474-6670(17)34383-5`.

[36] Deur J, Asgari J, Hrovat D. A dynamic tire friction model for combined longitudinal and lateral motion. InProceedings of the ASME-IMECE World Conference. 2001.

[37] Deur J, Asgari J, Hrovat D. A 3D Brush-type Dynamic Tire Friction Model. Vehicle Syst. Dyn. 2004;42(3):133-173. Available from: `https://doi.org/10.1080/00423110412331282887`.

[38] Deur J, Ivanovic V, Troulis M, Miano C, Hrovat D, Asgari J. Extensions of the LuGre tyre friction model related to variable slip speed along the contact patch length. Vehicle Syst. Dyn. 2005;43(supp):508-524. Available from: `https://doi.org/10.1080/00423110500229808`.

[39] Canudas-de-Wit C, Tsiotras P, Velenis E, Basset M, Gissinger G. Dynamic friction models for road/tire longitudinal interaction. Vehicle Syst. Dyn. 2003;39(3)189-226. Available from: `https://doi.org/10.1076/vesd.39.3.189.14152`.

[40] Tsiotras P, Velenis E, Sorine M. A LuGre Tire Friction Model With Exact Aggregate Dynamics. Vehicle Syst. Dyn. 2004;42(3):195-210. Available from: `https://doi.org/10.1080/00423110412331289835`.

[41] Velenis E, Tsiotras P, Canudas-de-Wit C, Sorine M. Dynamic tyre friction models for combined longitudinal and lateral vehicle motion. Vehicle Syst. Dyn. 2005;43(1):3-29. Available from: `https://doi.org/10.1080/00423110412331290464`.

[42] Pacejka HB, Besselink IJM. Magic Formula Tyre Model with Transient Properties. Vehicle System Dynamics. 1997;27(sup001)234-249. Available from: `https://doi.org/10.1080/00423119708969658`.

[43] Besselink IJM , Schmeitz AJC, Pacejka HB. (2010) An improved Magic Formula/Swift tyre model that can handle inflation pressure changes. Vehicle Syst. Dyn. 2010;48(S1):337-352. Available from: `https://doi.org/10.1080/00423111003748088`.

[44] Farroni F. T.R.I.C.K.-Tire/Road Interaction Characterization & Knowledge - A tool for the evaluation of tire and vehicle performances in outdoor test sessions. Mechanical Systems and Signal Processing. 2016;72-73:808-831. Available from: `https://doi.org/10.1016/j.ymssp.2015.11.019`.

[45] Farroni F, Sakhnevych A, Timpone F. Physical modelling of tire wear for the analysis of the influence of thermal and frictional effects on vehicle performance. Proceedings of the Institution of Mechanical Engineers, Part L: Journal of Materials: Design and Applications. 2017;231(1-2):151-161. Available from: `https://doi.org/10.1177/1464420716666107`.

[46] Farroni F, Sakhnevych A. Tire multiphysical modeling for the analysis of thermal and wear sensitivity on vehicle objective dynamics and racing performances. Simulation Modelling Practice and Theory 117 (2022).

[47] C. Canudas de Wit, H. Olsson, K. J. Astrom and P. Lischinsky, "A new model for control of systems with friction," in IEEE Transactions on Automatic Control, vol. 40, no. 3, pp. 419-425, March 1995, doi: 10.1109/9.376053.

[48] Schlippe B von, Dietrich R. Das flattern eined bepneuten rades. Bericht 140 der Lilienthal Gesellschaft. 1941: NACA TM 1365.

[49] Force and moment response of pneumatic tires to lateral motion inputs. Transaction ASME, Journal of Engineering for Industry, 88B. 1966.

[50] Pacejka HB. The wheel shimmy phenomenon: A theoretical and experimental investigation with particular reference to the non-linear problem [doctoral thesis]. Delft; 1966.

[51] M. Gafvert and J. Svendenius, "A novel semi-empirical tyre model for combined slips," Vehicle System Dynamics, vol. 43, no. 5, pp. 351–384, 2005.

[52] F. Bai, K. Guo, and D. Lu, "Tire model for turn slip properties," SAE International Journal of Commercial Vehicles, vol. 6, no. 2, pp. 353–361, 2013.

[53] N. Xu, K. Guo, X. Zhang, and H. R. Karimi, "An analytical tire model with flexible carcass for combined slips," Mathematical Problems in Engineering, vol. 2014, Article ID 397538, 9 pages, 2014.

[54] Takács D, Orosz G, Stépán G. Delay effects in shimmy dynamics of wheels with stretched string-like tyres. European Journal of Mechanics - A/Solids. 2009;28(3):516-525.

[55] Takács D, Stépán G. Micro-shimmy of towed structures in experimentally uncharted unstable parameter domain. Vehicle Syst. Dyn. 2012;50(11):1613-1630.

[56] Takács D, Stépán G, Hogan SJ. Isolated large amplitude periodic motions of towed rigid wheels. Nonlinear Dyn. 2008;52:27–34. Available from: `https://doi.org/10.1007/s11071-007-9253-y`.

[57] Takács D, Stépán G. Experiments on quasiperiodic wheel shimmy. ASME. J. Comput. Nonlinear Dynam. 2009;4(3):031007. Available from: `https://doi.org/10.1115/1.3124786`.

[58] Takács D, Stépán G. Contact patch memory of tyres leading to lateral vibrations of four-wheeled vehicles. Phil. Trans. R. Soc. A.37120120427. 2013. Available from: `http://doi.org/10.1098/rsta.2012.0427`

[59] S. Beregi, D. Takács, G. Stépán, Tyre induced vibrations of the car–trailer system, Journal of Sound and Vibration, Volume 362, 2016, Pages 214-227.

[60] Beregi, S., Takács, D. and Hős, C. Nonlinear analysis of a shimmying wheel with contact-force characteristics featuring higher-order discontinuities. Nonlinear Dyn 90, 877–888 (2017). Available from: https://doi.org/10.1007/s11071-017-3699-3.

[61] Beregi, S., Takacs, D., Gyebroszki, G. et al. Theoretical and experimental study on the nonlinear dynamics of wheel-shimmy. Nonlinear Dyn 98, 2581–2593 (2019). Available from: https://doi.org/10.1007/s11071-019-05225-w.

[62] Beregi, S., Takacs, D. and Stepan, G. Bifurcation analysis of wheel shimmy with non-smooth effects and time delay in the tyre–ground contact. Nonlinear Dyn 98, 841–858 (2019). Available from: https://doi.org/10.1007/s11071-019-05123-1.

[63] Beregi, S., Takács, D. Analysis of the tyre–road interaction with a non-smooth delayed contact model. Multibody Syst Dyn 45, 185–201 (2019). Available from: https://doi.org/10.1007/s11044-018-09636-2.

[64] O'Neill A, Gruber P, Watts JF, Prins J. Predicting Tyre Behaviour on Different Road Surfaces. In: Klomp M, Bruzelius F, Nielsen J, Hillemyr A. (eds) Advances in Dynamics of Vehicles on Roads and Tracks. IAVSD 2019. Lecture Notes in Mechanical Engineering. Springer, Cham. Available from: https://doi.org/10.1007/978-3-030-38077-9_215.

[65] O'Neill A, Prins J, Watts JF, Gruber P. Enhancing brush tyre model accuracy through friction measurements. Vehicle Syst. Dyn. 2021; pag. 1-23. Available from: https://doi.org/10.1080/00423114.2021.1893766.

[66] Duvaut G, Lions JL. Inequalities in Mechanics and Physics. Springer-Verlag: Berlin Heidelberg; 1976. Available from: https://doi.org/10.1007/978-3-642-66165-5.

[67] Kalker JJ. Variational Principles of Contact Elastostatics. J. Inst. Maths. Applics. 1997;20:199-219.

[68] Persson BNJ. Theory of rubber friction and contact mechanics. The Journal of Chemical Physics 2001;115(8):3840-3861. Available from: https://doi.org/10.1063/1.1388626.

[69] Persson BNJ, Albohr O, Tartaglino U, Volokitin AI, Tosatti E. On the nature of surface roughness with application to contact mechanics, sealing, rubber friction and adhesion. Journal of Physics: Condensed Matter 20004;17(1):R1-R62.

[70] Persson BNJ. Contact mechanics for randomly rough surfaces. Surface Science Reports. 2006;61(4):201-227. Available from: https://doi.org/10.1016/j.surfrep.2006.04.001.

[71] Goryacheva IG. Contact Mechanics in Tribology. 1st ed. Springer Dordrecht (1998). Available from: https://doi.org/10.1007/978-94-015-9048-8.

[72] Heinrich G, Klüppel M. Rubber friction, tread deformation and tire traction. Wear. 2008;265(7-8):1052-1060. Available from: https://www.sciencedirect.com/science/article/pii/S0043164808000847.

[73] Sakhnevych A. Multiphysical MF-based tyre modelling and parametrisation for vehicle setup and control strategies optimisation. Vehicle Syst. Dyn. 2021; pages 1-22. Available from: https://www.tandfonline.com/doi/full/10.1080/00423114.2021.1977833.

[74] Limebeer DJN, Massaro M. Dynamics and Optimal Control of Road Vehicle. Croydon: Oxford University Press; 2018.

[75] Romano L, Bruzelius F Jacobson B. Brush tyre models for large camber angles and steering speeds. Vehicle System Dynamics, 60:4, 1341-1392. Available from: https://doi.org/10.1080/00423114.2020.1854320.

[76] Romano L, Timpone F, Bruzelius F, Jacobson B. Analytical results in transient brush tyre models: theory for large camber angles and classic solutions with limited friction. Meccanica 57, 165-191 (2022). Available from: http://dx.doi.org/10.1007/s11012-021-01422-3.

[77] Romano L, Bruzelius F, Jacobson B. An extended LuGre-brush tyre model for large camber angles and turning speeds, Vehicle Syst. Dyn. 2022. Available from: https://doi.org/10.1080/00423114.2022.2086887.

[78] Romano L, Timpone F, Bruzelius F, Jacobson B. Rolling, tilting and spinning spherical wheels: analytical results using the brush theory. Mechanism and Machine Theory 173 (2022). Available from: https://doi.org/10.1016/j.mechmachtheory.2022.104836.

[79] Zegelaar PWA. The dynamic response of tyres to brake torque variations and road unevenesses [doctoral thesis]. Delft; 1998. Available from: http://resolver.tudelft.nl/uuid:c623e3fc-b88a-4bec-804a-10bcb7e94124.

[80] Evans LC. Partial differential equations. 2nd ed. American Mathematical Society; 1996.

[81] Ockendon JR, Howison S, Lacey A, Movchan A. Applied partial differential equations. Oxford

University Press; 2003.

[82] Polyanin AD, Manzhirov AV. Handbook of mathematics for engineers and scientists. Boca Raton–London: Chapman & Hall/CRC Press; 2007.

[83] Larsson S, Thomee V. Partial Differential Equations with Numerical Methods. 1st ed. Springer, Berlin, Heidelberg. 2009. Available from: https://doi.org/10.1007/978-3-540-88706-5.

[84] Karafyllis I, Krstic M. Input-to-State Stability for PDEs, Springer 2018.

[85] Debnath L, Mikusinski P. Introduction to Hilbert Spaces with applications. Elsevier. 3rd ed. (2005).

A Proofs

The mathematical proofs for the results advocated in the paper are given here.

A.1 Proofs for Sect. 3

This Appendix gives the proofs for Sect. 3. The first proof presented here is that of Theorem 3.1.

Proof of Theorem 3.1. The transformation $\tilde{\boldsymbol{u}}_{\boldsymbol{t}}(\xi,s) = [\tilde{u}_x(\xi,s)\ \tilde{u}_y(\xi,s)]^{\mathrm{T}} \triangleq \exp(-\rho s\mathbf{I})\boldsymbol{u}_{\boldsymbol{t}}(\xi,s)$, with $\rho \in \mathbb{R}_{>0}$ to be defined, turns the original PDEs (39) into

$$\frac{\partial \tilde{\boldsymbol{u}}_{\boldsymbol{t}}(\xi,s)}{\partial s} + \frac{\partial \tilde{\boldsymbol{u}}_{\boldsymbol{t}}(\xi,s)}{\partial \xi} = -\rho\tilde{\boldsymbol{u}}_{\boldsymbol{t}}(\xi,s) + \left(\mathbf{I} + 2a\mathbf{S}'\mathbf{K}_{\boldsymbol{t}}\right)^{-1}\left[\exp(-\rho s)\boldsymbol{\sigma}(s) + \mathbf{S}'\mathbf{K}_{\boldsymbol{t}}\tilde{\boldsymbol{u}}_{\boldsymbol{t}}(2a,s)\right]$$
$$+ \exp(-\rho s)\tilde{\mathbf{I}}\begin{bmatrix} a - \xi \\ 0 \end{bmatrix}\varphi(s), \qquad (\xi,s) \in \mathring{\mathscr{P}} \times (0,S), \tag{68}$$

with BC and IC given respectively by

$$\text{BC:} \qquad \tilde{\boldsymbol{u}}_{\boldsymbol{t}}(0,s) = \boldsymbol{0}, \qquad s \in (0,S), \tag{69a}$$

$$\text{IC:} \qquad \tilde{\boldsymbol{u}}_{\boldsymbol{t}}(\xi,0) = \boldsymbol{u}_{\boldsymbol{t}0}(\xi), \qquad \xi \in \mathring{\mathscr{P}}. \tag{69b}$$

Integrating Eq. (68) along the characteristic lines yields the following integral solution:

$$\tilde{\boldsymbol{u}}_{\boldsymbol{t}}(\xi,s) = \left(\boldsymbol{R}(\tilde{\boldsymbol{u}}_{\boldsymbol{t}})\right)(\xi,s) \triangleq \int_{\max(\xi-s,0)}^{\xi} \left(\mathbf{I} + 2a\mathbf{S}'\mathbf{K}_{\boldsymbol{t}}\right)^{-1}\mathbf{S}'\mathbf{K}_{\boldsymbol{t}}\exp\left(-\rho(\xi-\xi')\right)\tilde{\boldsymbol{u}}_{\boldsymbol{t}}\left(2a,\xi'-\xi+s\right)\mathrm{d}\xi'$$

$$+ \int_{\max(\xi-s,0)}^{\xi} \left(\mathbf{I} + 2a\mathbf{S}'\mathbf{K}_{\boldsymbol{t}}\right)^{-1}\exp(-\rho s)\boldsymbol{\sigma}\left(\xi'-\xi+s\right)\mathrm{d}\xi'$$

$$+ \int_{\max(\xi-s,0)}^{\xi} \tilde{\mathbf{I}}\begin{bmatrix} a - \xi' \\ 0 \end{bmatrix}\exp(-\rho s)\varphi\left(\xi'-\xi+s\right)\mathrm{d}\xi'$$

$$+ \boldsymbol{u}_{\boldsymbol{t}0}\left(\max(\xi-s,0)\right)\exp\left(-\rho\left(\xi-\max(\xi-s,0)\right)\right), \quad (\xi,s) \in \mathscr{P} \times [0,S], \tag{70}$$

or alternatively in components

$$\tilde{u}_x(\xi,s) = \left(R_x(\tilde{u}_x)\right)(\xi,s) \triangleq \int_{\max(\xi-s,0)}^{\xi} \frac{k_x}{C'_x + 2ak_x}\exp\left(-\rho(\xi-\xi')\right)\tilde{u}_x\left(2a,\xi'-\xi+s\right)\mathrm{d}\xi'$$

$$+ \int_{\max(\xi-s,0)}^{\xi} \frac{C'_x}{C'_x + 2ak_x}\exp(-\rho s)\sigma_x\left(\xi'-\xi+s\right)\mathrm{d}\xi'$$

$$+ u_{x0}\left(\max(\xi-s,0)\right)\exp\left(-\rho\left(\xi-\max(\xi-s,0)\right)\right), \quad (\xi,s) \in \mathscr{P} \times [0,S], \tag{71a}$$

$$\tilde{u}_y(\xi, s) = \big(R_y(\tilde{u}_y)\big)(\xi, s) \triangleq \int_{\max(\xi-s,0)}^{\xi} \frac{k_y}{C_y' + 2ak_y} \exp\Big(-\rho(\xi - \xi')\Big) \tilde{u}_y\big(2a, \xi' - \xi + s\big)\,\mathrm{d}\xi'$$

$$+ \int_{\max(\xi-s,0)}^{\xi} \frac{C_y'}{C_y' + 2ak_y} \exp(-\rho s)\sigma_y\big(\xi' - \xi + s\big)\,\mathrm{d}\xi'$$

$$+ \int_{\max(\xi-s,0)}^{\xi} \exp(-\rho s)\big(a - \xi'\big)\varphi\big(\xi' - \xi + s\big)\,\mathrm{d}\xi'$$

$$+ u_{y0}\big(\max(\xi - s, 0)\big) \exp\Big(-\rho\big(\xi - \max(\xi - s, 0)\big)\Big), \quad (\xi, s) \in \mathscr{P} \times [0, S]. \tag{71b}$$

Consider the metric spaces (M_x, d), (M_y, d), with M_x and M_y defined respectively as

$$M_x \triangleq \Big\{ \tilde{u}_x \in C^0(\mathscr{P} \times [0, S]; \mathbb{R}), \tilde{u}_x(\xi, 0) = u_{x0}(\xi) \Big\}, \tag{72a}$$

$$M_y \triangleq \Big\{ \tilde{u}_y \in C^0(\mathscr{P} \times [0, S]; \mathbb{R}), \tilde{u}_y(\xi, 0) = u_{y0}(\xi) \Big\}, \tag{72b}$$

and metric $d(\cdot, \cdot)$ induced by uniform norm $\sup_{s \in [0,S]} \|\cdot\|_\infty$, where the norm $\|\cdot\|_\infty$ is defined as $\|\cdot\|_\infty \triangleq \sup_{\xi \in \mathscr{P}} |\cdot|$, being the supremum interpreted as the essential supremum. It follows from the compatibility condition $\boldsymbol{u_{t0}}(0) = \boldsymbol{0}$ that the mappings $\tilde{u}_x \mapsto R_x(\tilde{u}_x)$, $\tilde{u}_y \mapsto R_y(\tilde{u}_y)$ are mappings from M_x and M_y onto themselves, respectively. The uniqueness of the proposed solutions in Eqs. (70) and (71) follows from Banach fixed point theorem [85], since $\tilde{u}_x \mapsto R_x(\tilde{u}_x)$, $\tilde{u}_y \mapsto R_y(\tilde{u}_y)$ are contractions for sufficiently large ρ. Indeed, for any $\tilde{\boldsymbol{u}}_{\boldsymbol{t}}^{\mathrm{I}}(\xi, s) = [\tilde{u}_x^{\mathrm{I}}(\xi, s)\ \tilde{u}_y^{\mathrm{I}}(\xi, s)]^{\mathrm{T}}$ and $\tilde{\boldsymbol{u}}_{\boldsymbol{t}}^{\mathrm{II}}(\xi, s) = [\tilde{u}_x^{\mathrm{II}}(\xi, s)\ \tilde{u}_y^{\mathrm{II}}(\xi, s)]^{\mathrm{T}}$,

$$\max_{\xi \in \mathscr{P}} \frac{k_x}{C_x' + 2ak_x} \Big| \tilde{u}_x^{\mathrm{I}}(2a, s) - \tilde{u}_x^{\mathrm{II}}(2a, s) \Big| \le L_x \Big\| \tilde{u}_x^{\mathrm{I}}(\cdot, s) - \tilde{u}_x^{\mathrm{II}}(\cdot, s) \Big\|_\infty, \tag{73a}$$

$$\max_{\xi \in \mathscr{P}} \frac{k_y}{C_y' + 2ak_y} \Big| \tilde{u}_y^{\mathrm{I}}(2a, s) - \tilde{u}_y^{\mathrm{II}}(2a, s) \Big| \le L_y \Big\| \tilde{u}_y^{\mathrm{I}}(\cdot, s) - \tilde{u}_y^{\mathrm{II}}(\cdot, s) \Big\|_\infty, \tag{73b}$$

which imply

$$\Big| \big(R_x(\tilde{u}_x^{\mathrm{I}})\big)(\xi, s) - \big(R_x(\tilde{u}_x^{\mathrm{II}})\big)(\xi, s) \Big| \le L_x \max_{s' \in [0,s]} \Big\| \tilde{u}_x^{\mathrm{I}}(\cdot, s') - \tilde{u}_x^{\mathrm{II}}(\cdot, s') \Big\|_\infty \int_{\max(\xi-s,0)}^{\xi} \exp\Big(-\rho(\xi - \xi')\Big)\,\mathrm{d}\xi'$$

$$\le \frac{L_x}{\rho} \max_{s' \in [0,S]} \Big\| \tilde{u}_x^{\mathrm{I}}(\cdot, s') - \tilde{u}_x^{\mathrm{II}}(\cdot, s') \Big\|_\infty, \quad (\xi, s) \in \mathscr{P} \times [0, S], \tag{74a}$$

$$\Big| \big(R_y(\tilde{u}_y^{\mathrm{I}})\big)(\xi, s) - \big(R_y(\tilde{u}_y^{\mathrm{II}})\big)(\xi, s) \Big| \le L_x \max_{s' \in [0,s]} \Big\| \tilde{u}_y^{\mathrm{I}}(\cdot, s') - \tilde{u}_y^{\mathrm{II}}(\cdot, s') \Big\|_\infty \int_{\max(\xi-s,0)}^{\xi} \exp\Big(-\rho(\xi - \xi')\Big)\,\mathrm{d}\xi'$$

$$\le \frac{L_y}{\rho} \max_{s' \in [0,S]} \Big\| \tilde{u}_y^{\mathrm{I}}(\cdot, s') - \tilde{u}_y^{\mathrm{II}}(\cdot, s') \Big\|_\infty, \quad (\xi, s) \in \mathscr{P} \times [0, S]. \tag{74b}$$

Finally, recalling the substitution $\tilde{\boldsymbol{u}}_{\boldsymbol{t}}(\xi, s) = \exp(-\rho s \mathbf{I})\boldsymbol{u_t}(\xi, s)$, splitting the integrals in Eq. (70), and defining $\boldsymbol{u_t}^-(\xi, s)$ and $\boldsymbol{u_t}^+(\xi, s)$ as in Eq. (23) provides (30). $\qquad \square$

The second proof is that of Proposition 3.1.

Proof of Proposition 3.1. In scalar form, Eqs. (22) and (23) satisfy the estimates

$$\big\| u_x(\cdot, s) \big\|_\infty \le \max_{s' \in [s-\xi, s]} 2a \big| \sigma_x(s') \big| \le \max_{s' \in [s-2a, s]} 2a \big| \sigma_x(s') \big|, \tag{75a}$$

$$\big\| u_y(\cdot, s) \big\|_\infty \le \max_{s' \in [s-\xi, s]} \bigg(2a \big| \sigma_y(s') \big| + \frac{a^2}{2} \big| \varphi(s') \big| \bigg) \le \max_{s' \in [s-2a, s]} \bigg(2a \big| \sigma_y(s') \big| + \frac{a^2}{2} \big| \varphi(s') \big| \bigg), \tag{75b}$$

for $s > 2a$, and

$$\big\| u_x(\cdot, s) \big\|_\infty \le \max_{s' \in [0,s]} 2a \big| \sigma_x(s') \big| + \big\| u_{x0}(\cdot) \big\|_\infty, \tag{76a}$$

32

$$\left\|u_y(\cdot,s)\right\|_\infty \le \max_{s'\in[0,s]}\left(2a\left|\sigma_y(s')\right| + \frac{a^2}{2}\left|\varphi(s')\right|\right) + \left\|u_{y0}(\cdot)\right\|_\infty, \tag{76b}$$

for $s \le 2a$. Combining (75) and (76), the result follows. $\qquad\square$

The third and last proof for Sect. 3 is that of Lemma 3.1.

Proof of Lemma 3.1. With similar arguments as in the Proof of Proposition 3.1, it may be deduced that

$$\left\|u_x(\cdot,s)\right\|_\infty \le \left\|u_{x0}(\cdot)\right\|_\infty \mathrm{e}^{-\rho(s-2a)} + \max_{s'\in[0,s]}\left(\frac{2ak_x}{C'_x + 2ak_x}\left\|u_x(\cdot,s')\right\|_\infty + \frac{2aC'_x}{C'_x + 2ak_x}\left|\sigma_x(s')\right|\right), \quad s \in \mathbb{R}_{\ge 0}, \tag{77a}$$

$$\begin{aligned}
\left\|u_y(\cdot,s)\right\|_\infty \le &\left\|u_{y0}(\cdot)\right\|_\infty \mathrm{e}^{-\rho(s-2a)} \\
&+ \max_{s'\in[0,s]}\left(\frac{2ak_y}{C'_y + 2ak_y}\left\|u_y(\cdot,s')\right\|_\infty + \frac{2aC'_y}{C'_y + 2ak_y}\left|\sigma_y(s')\right| + \frac{a^2}{2}\left|\varphi(s')\right|\right), \quad s \in \mathbb{R}_{\ge 0}.
\end{aligned} \tag{77b}$$

Therefore, Lemma 7.1 in [84] ensures that for every ρ, a, and $\varepsilon \in \mathbb{R}_{>0}$ there exist $\eta \in (0,\rho)$ such that

$$\begin{aligned}
\left\|u_x(\cdot,s)\right\|_\infty \mathrm{e}^{\eta s} \le &\left\|u_{x0}(\cdot)\right\|_\infty \mathrm{e}^{2\rho a} \\
&+ (1+\varepsilon)\max_{s'\in[0,s]}\left(\frac{2ak_x}{C'_x + 2ak_x}\left\|u_x(\cdot,s')\right\|_\infty + \frac{2aC'_x}{C'_x + 2ak_x}\left|\sigma_x(s')\right|\right)\mathrm{e}^{\eta s'}, \quad s \in \mathbb{R}_{\ge 0},
\end{aligned} \tag{78a}$$

$$\begin{aligned}
\left\|u_y(\cdot,s)\right\|_\infty \mathrm{e}^{\eta s} \le &\left\|u_{y0}(\cdot)\right\|_\infty \mathrm{e}^{2\rho a} \\
&+ (1+\varepsilon)\max_{s'\in[0,s]}\left(\frac{2ak_y}{C'_y + 2ak_y}\left\|u_y(\cdot,s')\right\|_\infty + \frac{2aC'_y}{C'_y + 2ak_y}\left|\sigma_y(s')\right| + \frac{a^2}{2}\left|\varphi(s')\right|\right)\mathrm{e}^{\eta s'}, \\
&s \in \mathbb{R}_{\ge 0},
\end{aligned} \tag{78b}$$

which in turn yield

$$\max_{s'\in[0,s]}\left\|u_x(\cdot,s')\right\|_\infty \mathrm{e}^{\eta s'} \le \frac{C'_x + 2ak_x}{C'_x - 2\varepsilon ak_x}\left\|u_{x0}(\cdot)\right\|_\infty \mathrm{e}^{2\rho a} + (1+\varepsilon)\max_{s'\in[0,s]}\frac{2aC'_x}{C'_x - 2\varepsilon ak_x}\left|\sigma_x(s')\right|\mathrm{e}^{\eta s'}, \quad s \in \mathbb{R}_{\ge 0}, \tag{79a}$$

$$\begin{aligned}
\max_{s'\in[0,s]}\left\|u_y(\cdot,s')\right\|_\infty \mathrm{e}^{\eta s'} \le &\frac{C'_y + 2ak_y}{C'_y - 2\varepsilon ak_y}\left\|u_{y0}(\cdot)\right\|_\infty \mathrm{e}^{2\rho a} \\
&+ (1+\varepsilon)\max_{s'\in[0,s]}\left(\frac{2aC'_y}{C'_y - 2\varepsilon ak_y}\left|\sigma_y(s')\right| + \frac{a^2(C'_y + 2ak_y)}{2(C'_y - 2\varepsilon ak_y)}\left|\varphi(s')\right|\right)\mathrm{e}^{\eta s'}, \quad s \in \mathbb{R}_{\ge 0}.
\end{aligned} \tag{79b}$$

Combining Eqs. (79) and (79) yields the desired result. $\qquad\square$

A.2 Proofs for Sect. 4

The only proof given here is that for Theorem 4.2.

Proof of Theorem 4.2. The transformations $\tilde{\boldsymbol{F}}_{\boldsymbol{t}} = [\tilde{F}_x(s)\ \tilde{F}_y(s)]^\mathrm{T} \triangleq \exp(-\rho s\mathbf{I})\boldsymbol{F}_{\boldsymbol{t}}(s)$ and $\tilde{\boldsymbol{z}} = [\tilde{z}_x(\xi,s)\ \tilde{z}_y(\xi,s)]^\mathrm{T} \triangleq \exp(-\rho s\mathbf{I})\boldsymbol{z}(\xi,s)$, with $\rho \in \mathbb{R}_{>0}$ to be defined, turn the original ODEs and PDEs (52) into the following system:

$$\frac{\mathrm{d}\tilde{\boldsymbol{F}}_{\boldsymbol{t}}(s)}{\mathrm{d}s} = -\rho\tilde{\boldsymbol{F}}_{\boldsymbol{t}}(s) + \exp(-\rho s)\hat{\boldsymbol{F}}_{\boldsymbol{t}}^{\mathrm{II}}\big(\exp(\rho s)\tilde{\boldsymbol{F}}_{\boldsymbol{t}}(s), \exp(\rho s)\tilde{\boldsymbol{z}}(\cdot,s), s\big), \quad s \in (0,S), \tag{80a}$$

$$\begin{aligned}
\frac{\partial\tilde{\boldsymbol{z}}(\xi,s)}{\partial s} + \frac{\partial\tilde{\boldsymbol{z}}(\xi,s)}{\partial\xi} = &-\left[\rho\mathbf{I} + \frac{\hat{v}_\mu(s)}{V_\mathrm{r}(s)g(\hat{v}_\mu(s))}\mathbf{C}_0\right]\tilde{\boldsymbol{z}}(\xi,s) + \exp(-\rho s)\boldsymbol{\sigma}(s) + \exp(-\rho s)\tilde{\mathbf{I}}\begin{bmatrix}a - \xi \\ 0\end{bmatrix}\varphi(s) \\
&- \exp(-\rho s)\mathbf{S}'\hat{\boldsymbol{F}}_{\boldsymbol{t}}^{\mathrm{II}}\big(\exp(\rho s)\tilde{\boldsymbol{F}}_{\boldsymbol{t}}(s), \exp(\rho s)\tilde{\boldsymbol{z}}(\cdot,s), s\big), \quad (\xi,s) \in \mathring{\mathscr{P}} \times (0,S),
\end{aligned} \tag{80b}$$

with BC and IC given respectively by

<div style="text-align:center">

BC: $\quad\tilde{\boldsymbol{z}}(0,s)=\mathbf{0}, \quad\quad\quad s\in(0,S),$ (81a)

IC: $\quad\tilde{\boldsymbol{z}}(\xi,0)=\boldsymbol{z}_0(\xi), \quad\quad\quad \xi\in\mathring{\mathscr{P}}, \quad\quad\quad \tilde{\boldsymbol{F}}_{\boldsymbol{t}}(0)=\boldsymbol{F}_{\boldsymbol{t}0}.$ (81b)

</div>

Integrating Eq. (80a) with respect to the travelled distance s and Eq. (80b) along the characteristic lines yields, respectively

$$
\begin{aligned}
\tilde{z}_x(\xi,s) &= \big(R_{1x}(\tilde{z}_x,\tilde{F}_x)\big)(\xi,s) \triangleq \int_{\max(\xi-s,0)}^{\xi}\exp\!\left(-\rho s-\int_{\xi'}^{\xi}\varphi_x\big(\tilde{\xi}-\xi+s\big)\,\mathrm{d}\tilde{\xi}\right)\sigma_x\big(\xi'-\xi+s\big)\,\mathrm{d}\xi'\\
&\quad -\int_{\max(\xi-s,0)}^{\xi}\exp\!\left(-\rho s-\int_{\xi'}^{\xi}\varphi_x\big(\tilde{\xi}-\xi+s\big)\,\mathrm{d}\tilde{\xi}\right)S_x'\hat{G}_x\big(\tilde{F}_x,\tilde{z}_x,\xi'-\xi+s\big)\,\mathrm{d}\xi'\\
&\quad +z_{x0}\big(\max(\xi-s,0)\big)\exp\!\left(-\int_{\max(\xi-s,0)}^{\xi}\big(\varphi_x\big(\xi'-\xi+s\big)+\rho\big)\,\mathrm{d}\xi'\right), \quad (\xi,s)\in\mathscr{P}\times[0,S],
\end{aligned}
$$

(82a)

$$
\begin{aligned}
\tilde{z}_y(\xi,s) &= \big(R_{1y}(\tilde{z}_y,\tilde{F}_y)\big)(\xi,s) \triangleq \int_{\max(\xi-s,0)}^{\xi}\exp\!\left(-\rho s-\int_{\xi'}^{\xi}\varphi_y\big(\tilde{\xi}-\xi+s\big)\,\mathrm{d}\tilde{\xi}\right)\sigma_y\big(\xi'-\xi+s\big)\,\mathrm{d}\xi'\\
&\quad \int_{\max(\xi-s,0)}^{\xi}\exp\!\left(-\rho s-\int_{\xi'}^{\xi}\varphi_y\big(\tilde{\xi}-\xi+s\big)\,\mathrm{d}\tilde{\xi}\right)(a-\xi')\varphi\big(\xi'-\xi+s\big)\,\mathrm{d}\xi'\\
&\quad -\int_{\max(\xi-s,0)}^{\xi}\exp\!\left(-\rho s-\int_{\xi'}^{\xi}\varphi_y\big(\tilde{\xi}-\xi+s\big)\,\mathrm{d}\tilde{\xi}\right)S_y'\hat{G}_y\big(\tilde{F}_y,\tilde{z}_y,\xi'-\xi+s\big)\,\mathrm{d}\xi'\\
&\quad +z_{y0}\big(\max(\xi-s,0)\big)\exp\!\left(-\int_{\max(\xi-s,0)}^{\xi}\big(\varphi_y\big(\xi'-\xi+s\big)+\rho\big)\,\mathrm{d}\xi'\right), \quad (\xi,s)\in\mathscr{P}\times[0,S],
\end{aligned}
$$

(82b)

and

$$
\begin{aligned}
\tilde{F}_x(s) &= \big(R_{2x}(\tilde{z}_x,\tilde{F}_x)\big)(s) \triangleq \exp(-\rho s)F_{x0}\\
&\quad +\int_0^s\exp\!\big(-\rho(s-s')\big)\exp(-\rho s')\hat{F}_x^{\mathrm{II}}\big(\exp(\rho s')\tilde{F}_x(s'),\exp(\rho s')\tilde{z}_x(\cdot,s'),s'\big)\,\mathrm{d}s', \quad s\in[0,S],
\end{aligned}
$$

(83a)

$$
\begin{aligned}
\tilde{F}_y(s) &= \big(R_{2y}(\tilde{z}_y,\tilde{F}_y)\big)(s) \triangleq \exp(-\rho s)F_{y0}\\
&\quad +\int_0^s\exp\!\big(-\rho(s-s')\big)\exp(-\rho s')\hat{F}_y^{\mathrm{II}}\big(\exp(\rho s')\tilde{F}_y(s'),\exp(\rho s')\tilde{z}_y(\cdot,s'),s'\big)\,\mathrm{d}s', \quad s\in[0,S],
\end{aligned}
$$

(83b)

where, for the sake of notation, the functions $\hat{\boldsymbol{G}}(\tilde{\boldsymbol{F}}_{\boldsymbol{t}},\tilde{\boldsymbol{z}},s)=[\hat{G}_x(\tilde{F}_x,\tilde{z}_x,s)\ \ \hat{G}_y(\tilde{F}_y,\tilde{z}_y,s)]^{\mathrm{T}}$ have been introduced in components as

$$
\hat{\boldsymbol{G}}\big(\tilde{\boldsymbol{F}}_{\boldsymbol{t}},\tilde{\boldsymbol{z}},s\big) \triangleq \hat{\boldsymbol{F}}_{\boldsymbol{t}}^{\mathrm{II}}\big(\exp(\rho s)\tilde{\boldsymbol{F}}_{\boldsymbol{t}}(\cdot,s),\exp(\rho s)\tilde{\boldsymbol{z}}(\cdot,s),s\big), \quad\quad (\xi,s)\in\mathscr{P}\times[0,S]. \tag{84}
$$

Now consider the complete metric spaces (M_x,d) and (M_y,d), with M_x and M_y defined respectively as

$$
M_x \triangleq \Big\{(\tilde{z}_x,\tilde{F}_x)\in C^0(\mathscr{P}\times[0,S];\mathbb{R})\times C^0([0,S];\mathbb{R}),\,\tilde{u}_x(\xi,0)=z_{x0}(\xi),\,\tilde{F}_x(0)=F_{x0}\Big\}, \tag{85a}
$$

$$
M_y \triangleq \Big\{(\tilde{z}_y,\tilde{F}_y)\in C^0(\mathscr{P}\times[0,S];\mathbb{R})\times C^0([0,S];\mathbb{R}),\,\tilde{u}_x(\xi,0)=z_{y0}(\xi),\,\tilde{F}_y(0)=F_{y0}\Big\}, \tag{85b}
$$

and metric $d(\cdot,\cdot)$ induced by the uniform norm $\sup_{s\in[0,S]}(\|\cdot\|_\infty+|\cdot|)$. It follows from the compatibility condition $\tilde{\boldsymbol{z}}_0(0)=\mathbf{0}$ that the mappings $(\tilde{z}_x,\tilde{F}_x)\mapsto(R_{1x}(\tilde{z}_x,\tilde{F}_x),R_{2x}(\tilde{z}_x,\tilde{F}_x))$, $(\tilde{z}_y,\tilde{F}_y)\mapsto(R_{1y}(\tilde{z}_y,\tilde{F}_y),R_{2y}(\tilde{z}_y,\tilde{F}_y))$ are mappings from M_x and M_y onto themselves, respectively. The uniqueness of the proposed solutions in Eqs. (82) and (83) follows from Banach fixed point theorem [85], since $(\tilde{z}_x,\tilde{F}_x)\mapsto(R_{1x}(\tilde{z}_x,\tilde{F}_x),R_{2x}(\tilde{z}_x,\tilde{F}_x))$,

$(\tilde{z}_y, \tilde{F}_y) \mapsto (R_{1y}(\tilde{z}_y, \tilde{F}_y), R_{2y}(\tilde{z}_y, \tilde{F}_y))$ are contractions for sufficiently large ρ. Indeed, for any $\boldsymbol{z}^{\mathrm{I}}(\xi, s) = [z_x^{\mathrm{I}}(\xi, s)\ z_y^{\mathrm{I}}(\xi, s)]^{\mathrm{T}}$, $\boldsymbol{z}^{\mathrm{II}}(\xi, s) = [z_x^{\mathrm{II}}(\xi, s)\ z_y^{\mathrm{II}}(\xi, s)]^{\mathrm{T}}$ and $\boldsymbol{F_t}^{\mathrm{I}}(s) = [F_x(s)^{\mathrm{I}}\ F_y(s)^{\mathrm{I}}]^{\mathrm{T}}$, $\boldsymbol{F_t}^{\mathrm{II}}(s) = [F_x(s)^{\mathrm{II}}\ F_y(s)^{\mathrm{II}}]^{\mathrm{T}}$,

$$\left|\hat{F}_x\big(F_x^{\mathrm{I}}(s), z_x^{\mathrm{I}}(\cdot, s), s\big) - \hat{F}_x\big(F_x^{\mathrm{II}}(s), z_x^{\mathrm{II}}(\cdot, s), s\big)\right| \leq L_x \left\|z_x^{\mathrm{I}}(\cdot, s) - z_x^{\mathrm{II}}(\cdot, s)\right\|_\infty + L_x \left|F_x^{\mathrm{I}}(s) - F_x^{\mathrm{II}}(s)\right|, \quad (86\mathrm{a})$$

$$\left|\hat{F}_y\big(F_y^{\mathrm{I}}(s), z_y^{\mathrm{I}}(\cdot, s), s\big) - \hat{F}_y\big(F_y^{\mathrm{II}}(s), z_y^{\mathrm{II}}(\cdot, s), s\big)\right| \leq L_y \left\|z_y^{\mathrm{I}}(\cdot, s) - z_y^{\mathrm{II}}(\cdot, s)\right\|_\infty + L_y \left|F_y^{\mathrm{I}}(s) - F_y^{\mathrm{II}}(s)\right|, \quad (86\mathrm{b})$$

with

$$L_x \triangleq \frac{C_x'}{F_z} \max\left\{ \max_{s \in [0,S]} \frac{1}{V_{\mathrm{r}}(s)\tilde{c}_x}, \ \max_{s \in [0,S]} \frac{c_{0x}}{V_{\mathrm{r}}(s)\tilde{c}_x} \left|1 - \frac{\hat{v}_\mu(s) c_{1x}}{g(\hat{v}_\mu(s))}\right| F_z + \frac{c_{1x} q_z(2a)}{\tilde{c}_x} + \frac{c_{1x}}{\tilde{c}_x} \int_0^{2a} \left|\frac{\mathrm{d}q_z(\xi)}{\mathrm{d}\xi}\right| \mathrm{d}\xi \right\},$$
$$(87\mathrm{a})$$

$$L_y \triangleq \frac{C_y'}{F_z} \max\left\{ \max_{s \in [0,S]} \frac{1}{V_{\mathrm{r}}(s)\tilde{c}_y}, \ \max_{s \in [0,S]} \frac{c_{0y}}{V_{\mathrm{r}}(s)\tilde{c}_y} \left|1 - \frac{\hat{v}_\mu(s) c_{1y}}{g(\hat{v}_\mu(s))}\right| F_z + \frac{c_{1y} q_z(2a)}{\tilde{c}_y} + \frac{c_{1y}}{\tilde{c}_y} \int_0^{2a} \left|\frac{\mathrm{d}q_z(\xi)}{\mathrm{d}\xi}\right| \mathrm{d}\xi \right\},$$
$$(87\mathrm{b})$$

where it has been defined $\tilde{c}_x \triangleq c_{1x} + c_{2x}$ and $\tilde{c}_y \triangleq c_{1y} + c_{2y}$. This also implies

$$\left|\big(R_{1x}(\tilde{z}_x^{\mathrm{I}}, \tilde{F}_x^{\mathrm{I}})\big)(\xi, s) - \big(R_{1x}(\tilde{z}_x^{\mathrm{II}}, \tilde{F}_x^{\mathrm{II}})\big)(\xi, s)\right|$$
$$\leq S_x' L_x \max_{s' \in [0,s]} \left(\left\|\tilde{z}_x^{\mathrm{I}}(\cdot, s') - \tilde{z}_x^{\mathrm{II}}(\cdot, s')\right\|_\infty + \left|\tilde{F}_x^{\mathrm{I}}(s') - \tilde{F}_x^{\mathrm{II}}(s')\right|\right)$$
$$\times \int_{\max(\xi-s,0)}^\xi \exp\left(-\rho(\xi - \xi') - \int_{\xi'}^\xi \varphi_x\big(\tilde{\xi} - \xi + s\big)\,\mathrm{d}\tilde{\xi}\right)\mathrm{d}\xi' \qquad (88\mathrm{a})$$
$$\leq \frac{S_x' L_x}{\rho} \max_{s' \in [0,s]} \left(\left\|\tilde{z}_x^{\mathrm{I}}(\cdot, s') - \tilde{z}_x^{\mathrm{II}}(\cdot, s')\right\|_\infty + \left|\tilde{F}_x^{\mathrm{I}}(s') - \tilde{F}_x^{\mathrm{II}}(s')\right|\right), \quad (\xi, s) \in \mathscr{P} \times [0, S],$$

$$\left|\big(R_{1y}(\tilde{z}_y^{\mathrm{I}}, \tilde{F}_y^{\mathrm{I}})\big)(\xi, s) - \big(R_{1y}(\tilde{z}_y^{\mathrm{II}}, \tilde{F}_y^{\mathrm{II}})\big)(\xi, s)\right|$$
$$\leq S_y' L_y \max_{s' \in [0,s]} \left(\left\|\tilde{z}_y^{\mathrm{I}}(\cdot, s') - \tilde{z}_y^{\mathrm{II}}(\cdot, s')\right\|_\infty + \left|\tilde{F}_y^{\mathrm{I}}(s') - \tilde{F}_y^{\mathrm{II}}(s')\right|\right)$$
$$\times \int_{\max(\xi-s,0)}^\xi \exp\left(-\rho(\xi - \xi') - \int_{\xi'}^\xi \varphi_y\big(\tilde{\xi} - \xi + s\big)\,\mathrm{d}\tilde{\xi}\right)\mathrm{d}\xi' \qquad (88\mathrm{b})$$
$$\leq \frac{S_y' L_y}{\rho} \max_{s' \in [0,s]} \left(\left\|\tilde{z}_y^{\mathrm{I}}(\cdot, s') - \tilde{z}_y^{\mathrm{II}}(\cdot, s')\right\|_\infty + \left|\tilde{F}_y^{\mathrm{I}}(s') - \tilde{F}_y^{\mathrm{II}}(s')\right|\right), \quad (\xi, s) \in \mathscr{P} \times [0, S],$$

and

$$\left|\big(R_{2x}(\tilde{z}_x^{\mathrm{I}}, \tilde{F}_x^{\mathrm{I}})\big)(s) - \big(R_{2x}(\tilde{z}_x^{\mathrm{II}}, \tilde{F}_x^{\mathrm{II}})\big)(s)\right|$$
$$\leq L_x \max_{s' \in [0,s]} \left(\left\|\tilde{z}_x^{\mathrm{I}}(\cdot, s') - \tilde{z}_x^{\mathrm{II}}(\cdot, s')\right\|_\infty + \left|\tilde{F}_x^{\mathrm{I}}(s') - \tilde{F}_x^{\mathrm{II}}(s')\right|\right) \int_0^s \exp\big(-\rho(s - s')\big)\,\mathrm{d}s' \qquad (89\mathrm{a})$$
$$\leq \frac{L_x}{\rho} \max_{s' \in [0,S]} \left(\left\|\tilde{z}_x^{\mathrm{I}}(\cdot, s') - \tilde{z}_x^{\mathrm{II}}(\cdot, s')\right\|_\infty + \left|\tilde{F}_x^{\mathrm{I}}(s') - \tilde{F}_x^{\mathrm{II}}(s')\right|\right), \quad s \in [0, S],$$

$$\left|\big(R_{2y}(\tilde{z}_y^{\mathrm{I}}, \tilde{F}_y^{\mathrm{I}})\big)(s) - \big(R_{2y}(\tilde{z}_y^{\mathrm{II}}, \tilde{F}_y^{\mathrm{II}})\big)(s)\right|$$
$$\leq L_y \max_{s' \in [0,s]} \left(\left\|\tilde{z}_y^{\mathrm{I}}(\cdot, s') - \tilde{z}_y^{\mathrm{II}}(\cdot, s')\right\|_\infty + \left|\tilde{F}_y^{\mathrm{I}}(s') - \tilde{F}_y^{\mathrm{II}}(s')\right|\right) \int_0^s \exp\big(-\rho(s - s')\big)\,\mathrm{d}s' \qquad (89\mathrm{b})$$
$$\leq \frac{L_y}{\rho} \max_{s' \in [0,S]} \left(\left\|\tilde{z}_y^{\mathrm{I}}(\cdot, s') - \tilde{z}_y^{\mathrm{II}}(\cdot, s')\right\|_\infty + \left|\tilde{F}_y^{\mathrm{I}}(s') - \tilde{F}_y^{\mathrm{II}}(s')\right|\right), \quad s \in [0, S].$$

Finally, recalling the substitutions $\tilde{\boldsymbol{F}}_{\boldsymbol{t}}(s) = \exp(-\rho s \mathbf{I})\boldsymbol{F_t}(s)$ and $\tilde{\boldsymbol{z}}(\xi, s) = \exp(-\rho s \mathbf{I})\boldsymbol{z}(\xi, s)$, and defining $\boldsymbol{z}^-(\xi, s)$ and $\boldsymbol{z}^+(\xi, s)$ as in Eq. (48) provides (55). $\qquad \square$